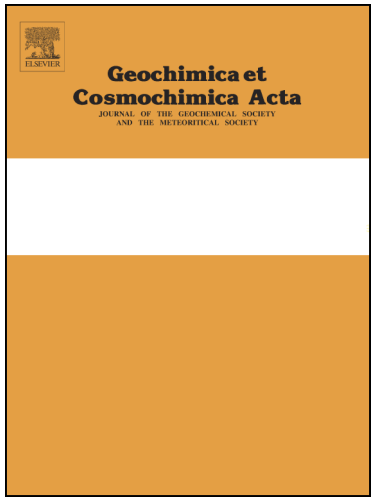

The role of sedimentology, oceanography, and alteration on the δ ^{56}Fe value of the Sokoman Iron Formation, Labrador Trough, Canada

Urmidola Raye, Peir K. Pufahl, T. Kurtis Kyser, Estelle Ricard, Eric E. Hiatt

PII: S0016-7037(15)00315-4
DOI: http://dx.doi.org/10.1016/j.gca.2015.05.020
Reference: GCA 9289

To appear in: *Geochimica et Cosmochimica Acta*

Received Date: 22 October 2014
Accepted Date: 10 May 2015

Please cite this article as: Raye, U., Pufahl, P.K., Kurtis Kyser, T., Ricard, E., Hiatt, E.E., The role of sedimentology, oceanography, and alteration on the δ ^{56}Fe value of the Sokoman Iron Formation, Labrador Trough, Canada, *Geochimica et Cosmochimica Acta* (2015), doi: http://dx.doi.org/10.1016/j.gca.2015.05.020

The role of sedimentology, oceanography, and alteration on the $\delta^{56}Fe$ value of the Sokoman Iron Formation, Labrador Trough, Canada

Urmidola Raye[1*], Peir K. Pufahl[2], T. Kurtis Kyser[1], Estelle Ricard[1], Eric E. Hiatt[3]

[1] Department of Geological Sciences and Geological Engineering, Queen's University, Kingston, Ontario K7L3N6, Canada
[2] Department of Earth and Environmental Science, Acadia University, Wolfville, Nova Scotia B4P2R6, Canada
[3] Department of Geology, University of Wisconsin – Oshkosh, Oshkosh, WI 54901, USA

[*]E-mail: raye@geol.queensu.ca

Abstract

The Sokoman Formation is a ca. 100-m-thick succession of interbedded iron formation and fine-grained siliciclastics deposited at 1.88 Ga. Accumulation occurred on a dynamic paleoshelf where oxygen stratification, coastal upwelling of hydrothermally derived Fe and Si, microbial processes, tide and storm currents, diagenesis, and low-grade prehnite-pumpellyite metamorphism controlled lithofacies character and produced complex associations of multigenerational chert, hematite, magnetite, greenalite, stilpnomelane and Fe carbonate. Hematite-rich facies were deposited along suboxic segments of the coastline where photosynthetic oxygen oases impinged on the seafloor. Hematitic, cross-stratified grainstones were formed by winnowing and reworking of freshly precipitated Fe-(oxyhydr)oxide and opal-A by waves and currents into subaqueous dunes. Magnetite-rich facies contain varying proportions of greenalite and stilpnomelane and record deposition in anoxic middle shelf environments beneath an oxygen chemocline. Minor negative Ce anomalies in hematitic facies, but prominent positive Ce and Eu anomalies and high LREE/HREE ratios in magnetite-rich facies imply the existence of a weakly oxygenated surface ocean above anoxic bottom waters.

The Fe isotopic composition of 31 whole rock ($-0.46 \leq \delta^{56}Fe \leq 0.47$‰) and 21 magnetite samples ($-0.29 \leq \delta^{56}Fe \leq 0.22$ ‰) from suboxic and anoxic lithofacies was controlled primarily by the physical oceanography of the paleoshelf. Despite low-grade metamorphism recorded by the $\delta^{18}O$ values of paragenetically related quartz and magnetite, the Sokoman Formation preserves a robust primary Fe isotopic signal. Coastal upwelling is interpreted to have affected

the isotopic equilibria between Fe^{2+}_{aq} and Fe-(oxyhydr)oxide in open marine versus coastal environments, which controlled the Fe isotopic composition of lithofacies. Unlike previous work that focuses on microbial and abiotic fractionation processes with little regard for paleoenvironment, our work demonstrates that depositional setting is paramount in governing the Fe isotopic composition of iron formations irrespective of what Fe-bearing minerals precipitated.

Keywords: Fe isotopes, Diagenesis, Sokoman Formation, Paleoproterozoic iron formation, Paleoceanography, Sequence stratigraphy

1. Introduction

Iron formation is a generally Precambrian, Fe-rich biochemical sedimentary rock that holds important clues to the evolution of the early ocean-atmosphere system (Gross, 1980, 1983; Simonson, 2003; Klein, 2005; Bekker et al., 2010; Pufahl, 2010). Exhalative iron formation is predominantly Archean and accumulated near spreading centers or island arcs (Gross, 1980, 1983; Pufahl, 2010). Continental margin iron formation is mostly Paleoproeterozoic having precipitated in association with upwelling of hydrothermally derived Fe and Si on the tectonically stable, unrimmed shelves that developed at the end of the Archean (Trendall, 2002; Simonson 2003; Trendall and Blockley, 2004; Klein, 2005; Bekker et al., 2010; Pufahl, 2010). These large deposits are economically important because they contain the majority of Fe for steel production (Clout and Simonson, 2005). Their appearance approximately coincides with changing ocean-atmosphere chemistry during the Great Oxidation Event (Kholodov and Butuzova 2004; Condie et al. 2001; Klein 2005; Reddy and Evans 2009; Bekker et al. 2010; Pufahl, 2010). Because some iron formation lithofacies are direct seawater precipitates, iron formation chemistry is often regarded as a robust proxy for the composition of the early oceans and, by inference, the early atmosphere.

However, almost all iron formations are now metamorphic rocks formed of altered lithofacies containing complex associations of chert, hematite, magnetite, Fe silicates, and Fe carbonates (Dauphas at al., 2004, 2007; Frost, 2007; Hyslop, 2008; Johnson et al., 2003; Steinhoefel et al., 2010). These mineralogical assemblages reflect a complicated paragenesis that controls iron formation chemistry. In spite of such multifaceted and varied depositional and post-

depositional histories, redox-sensitive trace elements (Cu, Cr, V, Cd, Mo, U, Y, Zn, and REEs) and the ratios of stable isotopes (δ^{56}Fe, δ^{53}Cr, $\delta^{97/95}$Mo, $\delta^{98/95}$Mo, δ^{34}S, and δ^{33}S) are routinely used to interpret the chemical evolution of Precambrian seawater (Pufahl and Hiatt, 2012; Pufahl et al., 2014).

The purpose of this paper is to interpret the petrography, mineralogy, geochemistry, and the δ^{56}Fe and δ^{18}O values of the 1.88 Ga Sokoman Iron Formation in a depositional, diagenetic, and metamorphic context. Such an approach permits assessment of whether geochemical and isotopic anomalies reflect conditions at the time of deposition or the result of subsequent alteration. The Sokoman Formation is a ca. 100-m-thick succession of interbedded iron formation and fine-grained siliciclastics that accumulated in the Labrador Trough of eastern Canada (Klein and Fink 1976; Klein, 1978; Pufahl et al., 2014). Deposition occurred on a dynamic paleoshelf where oxygen stratification, coastal upwelling, microbial processes, tide and storm currents, diagenesis, and prehnite-pumpellyite facies metamorphism controlled lithofacies character (Pufahl et al., 2014). Since the Sokoman Formation is only weakly metamorphosed, it is well suited for assessing the utility of using the δ^{56}Fe values of iron formation as a paleoenvironmental proxy.

2. Geological background

The Labrador Trough (Fig.1a) is a belt of sedimentary and volcanic rocks along the margin of the Paleoproterozoic supercontinent Columbia (Gross, 1968; Wardle and Bailey, 1981; Gross and Zajac, 1983; Clark and Wares, 2004; Evans and Mitchell, 2011; Edwards et al., 2012; Meert, 2012). Iron formation occurs only in the Sokoman Formation of the Ferriman Group, which in turn belongs to the Kaniapiskau Supergroup (Clark and Wares, 2006). The Kaniapiskau Supergroup is divided into three "cycles" of deposition recording a complete Wilson Cycle of rifting, drifting, and ocean closure. The Ferriman Group characterizes second cycle sedimentation during drifting, passive margin development and the onset of collision (Wardle et al., 2002). Accumulation of second cycle sediments began by ca. 1.88 Ga and telescoping of the margin started by ca. 1.87 Ga (Clark and Wares, 2004).

In the vicinity of Schefferville, Quebec, where this study is located, the Torngat (ca. 1.87 to 1.81) and New Quebec (ca. 1.82 to 1.77 Ga) orogenies affected the Ferriman Group to prehnite-pumpellyite facies metamorphism (Zajac, 1974; Klein and Fink, 1976; Dimroth and Dressler, 1978; Machado et al., 1997). Here, the Ferriman Group is parautochthonous and flat lying, preserving vertical and lateral lithofacies relations in a paleoenvironmental context. Higher grade metamorphism is restricted to the southern Labrador Trough where the Grenville Orogeny (ca. 1.0 Ga) intensely folded and buried Ferriman strata (Clark and Wares, 2006).

3. Ferriman Group

The Ferriman Group is subdivided from base to top into the Wishart, Nimish, Ruth, Sokoman, and Menihek formations (Fig.1b). The Wishart Formation is composed of sandstones that accumulated in a range of shelf environments (Chauvel and Dimroth, 1974; Simonson, 1984). Lagoonal mudstones, volcanics, and iron formation of the Ruth, Nimish, and Sokoman formations, respectively, form a sedimentologic succession in unconformable contact with the underlying Wishart and overlying Menihek formations (Pufahl et al., 2014). The Nimish Formation is interpreted to record episodes of transtensional volcanism on this otherwise passive margin (Findlay et al., 1995). Turbidites and shales of the Menihek Formation are thought to record foreland basin development during the onset of the Torngat Orogen (Hoffman, 1988).

3.1. Sokoman and Ruth formations

The Sokoman and Ruth formations comprise a ca. 100-m-thick succession of seven iron formation and siliciclastic lithofacies (Fig.2; Table 1of Pufahl et al., 2014). A U-Pb age of 1877.8 ± 1.3 Ma for the Sokoman Formation is derived from zircons in interbedded syenetic cobbles, which are geochemically identical to intercalated Nimish volcanics (Findlay et al., 1995). Vertical and lateral facies stacking patterns record deposition through two relative sea-level cycles that produced seven distinct lithofacies defining two unconformity-bounded sequences (Pufahl et al., 2014).

Sequence stratigraphy highlights facies relationships in a chronostratigraphic framework that links sedimentation and lithofacies chemistry to variations in accommodation and sediment

supply through time (e.g. Catuneanu et al., 2009). This approach provides the foundation for properly interpreting sedimentology, oceanography, microbial ecology, and geochemistry in paleoenvironmental, diagenetic, and metamorphic context (Pufahl and Hiatt, 2012).

Sequence 1 is 50 to 70 m. thick and records deposition of hematitic peritidal iron formation as deep as the upper shoreface (Pufahl et al., 2014). Its unconformable lower contact with the Wishart Formation is interpreted as a forced regression surface (Pufahl et al., 2014). Lowstand deposits are composed of lagoonal black shale (Facies F1, F2; Ruth Formation), stromatolites, and supratidal chert (Facies F3; Sokoman Formation) that are overlain by hematitic, tide and storm-deposited, granular iron formation of the transgressive systems tract (Facies F4; Sokoman Formation). Highstand deposits are characterized by subtidal, hematitic granular iron formation (Facies F4 & F6; Sokoman Formation).

Sequence 2 is 20 to 60-m-thick and rests unconformably on the highstand systems tract of Sequence 1 (Pufahl et al., 2014). The lowstand systems tract also contains supratidal chert (Facies 2; Sokoman Formation), but it is interbedded with hematitic, peritidal grainstones (Facies F3; Sokoman Formation) rather than lagoonal shale. The transgressive systems tract is a condensed, concretionary grainstone facies (Facies F5) interpreted to record seafloor cementation on a wave-swept transgressive surface. The rest of the transgressive systems tract reflects continued deepening and the deposition of magnetite- and Fe silicate-rich iron formation (Facies F7). This parallel-bedded facies reflects current- and wave-reworking of ripples and dunes above fair weather wave base (Pufahl et al., 2014).

Because the Ferriman Group experienced only very low-grade metamorphism, the change from a hematite-dominated nearshore to a magnetite- and Fe silicate-dominated offshore likely reflect differing redox conditions of bottom and pore water at the time of deposition rather than subsequent effects from metamorphism (Pufahl and Hiatt, 2012; Pufahl et al., 2014). Hematite is interpreted to record deposition in shallow suboxic environments where stromatolites produced photosynthetic oxygen oases that impinged on the seafloor. Freshly precipitated Fe-(oxyhydr)oxide was converted to hematite in suboxic pore water during burial (Klein, 2005). Accompanying the physiochemical precipitation of Fe-(oxyhydr)oxide in the water column via the oxidation of ferrous Fe by photosynthetic oxygen, preserved fossil microbial communities imply suboxic, bacterial precipitation (Edwards, 2012).

Laminated magnetite- and Fe silicate-rich facies are interpreted to reflect precipitation in anoxic settings (Pufahl et al., 2014). Authigenic magnetite probably formed when Fe-(oxyhydr)oxide precipitated in suboxic surface waters (Cloud, 1973; Pufahl, 2010) and incorporated ferrous Fe either from diffusion of overlying seawater or through bacterial dissimilatory Fe reduction (Laberge, 1964; Raiswell, 2006; Johnson et al., 2008 a,b). Petrographic data indicates that Fe silicates such as greenalite and stilpnomelane are also synsedimentary precipitates formed from primary Fe-rich silica gels that accumulated with Fe-(oxyhydr)oxide in anoxic settings (Klein, 2005; Pufahl et al., 2014).

The character and distribution of redox sensitive facies indicate that iron formation deposition was governed by a combination of shelf hydraulics, upwelling of hydrothermal Fe and Si, the ratio of Fe influx to precipitation as well as oxygen levels. The sharp transition from hematitic shallow-water facies to laminated magnetite-rich deposits indicates a prominent oxygen chemocline initially controlled iron formation mineralogy and chemistry. The development of a suboxic surface ocean is interpreted to reflect photosynthetic oxygen production from a combination of peritidal stromatolites and cyanobacterial phytoplankton in the offshore (Pufahl and Fralick, 2004; Pufahl, 2014).

4. Analytical methods

Forty-three polished thin sections were prepared from drill cores. Thin sections were studied under Nikon Type 104 transmitted and reflected light petrographic microscope to investigate paragenetic and textural relations among minerals. The mineralogical composition was confirmed by powder X-ray diffraction using a Panalytical X'Pert Pro powder diffractometer. All samples of representative thin sections and lithofacies were powdered using an electric alumina mortar grinder. One half of this powdered fraction was used for major, trace element and whole-rock iron (Fe) isotope ratio analysis. The other half was used for magnetite Fe isotope, magnetite and quartz oxygen (O) isotope ratio analysis. Magnetite separates from 21 samples were analyzed for Fe isotope ratios, 14 magnetites for O isotope ratios and quartz separates from 14 samples were analyzed for O isotope ratios. Magnetites were first magnetically separated using a hand magnet and then hand-picked. For quartz, the whole rock powdered fraction (355 -125 μm) was cleaned with concentrated HCl and Milli-Q water (18.2 MΩ cm) and

minerals were hand-picked under optical microscope. Major and trace elements were analysed by inductively coupled plasma optical emission spectrometry (iCAP 6000 ICP-OES, Thermo Scientific) and high resolution inductively coupled plasma mass spectrometer (ELEMENT HR-ICP-MS, Thermo Scientific) respectively. All analyses were performed at the Queen's Facility for Isotope Research (QFIR).

4.1. Iron isotope analysis

Whole rock powdered samples (0.05 g) as well as magnetite separates (0.01 g) were completely digested in Teflon beakers using concentrated acids in a class 100 clean lab. Chemical purification was undertaken using procedures outlined by Borrok et al., (2007) with anion exchange chromatography using Bio-Rad polypropylene column (length 8 cm, internal diameter 0.4 cm) filled with 1 ml of Bio-Rad AG MP-1(100-200 mesh, chloride form) resin and HCl conditioning. Samples were loaded and the matrix eluted in 4 ml of 10M HCl and 7 ml of 5M HCl. Iron was eluted in 4ml of 1M HCl. Iron extraction yields were 100 ± 3%. The Fe isotopic composition was measured in 2% HNO_3 at a concentration of 3 ppm on a Thermo-Finnigan Neptune MC-ICP-MS (45 V on ^{56}Fe) in medium and high-resolution mode. Nickel was used as an internal standard for mass bias correction whose concentration in final solution was also 3 ppm.

A standard-sample-standard bracketing method was used for mass bias and instrument drift correction and Fe isotopic compositions are reported in standard delta (δ) notation in per mil (‰) relative to a standard: $\delta^{56}Fe = [((^{56}Fe/^{54}Fe)_{sample}/(^{56}Fe/^{54}Fe)_{standard}) - 1]\times10^3$, where $(^{56}Fe/^{54}Fe)_{standard}$ is represented by IRMM-014 (Taylor et al., 1992) standard with a $\delta^{56}Fe$ value of –0.09 ± 0.05‰ on the igneous rock scale (Beard et al., 2003). A magnetite in-house standard was used as matrix matching standard for Fe isotope analysis. The geostandard IF-G (Centre de Recherches Petrographiques et Geochimiques, CNRS, B.P. 20, Vandoeuvre-lès-Nancy Cedex 54501) was dissolved several times and processed through ion-exchange columns for each aliquot. A $\delta^{56}Fe$ value of 0.64 ±0.03 ‰ was obtained (n = 12), which is within the average of previously reported values (0.58 - 0.67 ‰ IRMM, GeoReM). Measured $\delta^{56}Fe$ and $\delta^{57}Fe$ values followed a mass dependent relation ($\delta^{57}Fe = 1.5\pm0.2$‰). The internal precision of each Fe isotope analysis was typically better than 0.09‰ (2SE) for whole rock and better than 0.04‰

(2SE) for magnetites. External precision was better than ±0.03‰ in $\delta^{56}Fe$ based on repeat analysis of the same magnetites and whole-rock samples.

4.2. Oxygen isotopic analysis

Oxygen isotope analyses of magnetite and quartz separates were done following the method of Clayton and Mayeda (1963). Approximately 5 mg of powdered minerals were reacted in bromine pentafluoride (BrF_5) atmosphere at 550°C and 650°C overnight for quartz and magnetite, respectively. The extracted oxygen was converted to CO_2 in contact with a heated graphite rod and cryogenically collected CO_2 was then analyzed off-line using a Finnigan MAT 252 isotope ratio mass spectrometer (IRMS). The analytical precision of $\delta^{18}O$ is better than 0.1 per mil. Oxygen isotopic compositions are reported in standard delta (δ) notation in per mil (‰) relative to Vienna Standard Mean Ocean Water (VSMOW): $\delta^{18}O = [(({}^{18}O/{}^{16}O)_{sample}/ ({}^{18}O/{}^{16}O)_{VSMOW}) - 1] \times 10^3$.

5. Results

5.1. Petrography and paragenesis

Petrographic and X-ray diffraction analysis indicates that lithofacies are composed of complex associations of multigenerational chert, hematite, magnetite, greenalite, stilpnomelane and Fe carbonates such as ankerite and siderite. Textural relationships between minerals confirm that this assemblage defines two redox sensitive, paragenetic pathways that controlled iron formation chemistry (Fig. 3). The suboxic paragenetic pathway is characterized by hematite and chert-rich, laminated and granular iron formation (Fig. 4 A, B, C; Facies F3, F4, F5) that accumulated in shallow stromatolitic environments enriched in photosynthetic oxygen (Pufahl et al., 2014). Laminated iron formation is formed of microcrystalline chert with disseminated subhedral hematite crystals (Fig. 4A; Facies F3). It reflects the rain of Fe-(oxyhydr)oxide and opal-A (hydrated amorphous silica) precipitated in a suboxic water column. Along energetic segments of the coastline these hematitic and siliceous muds were reworked by tides and storms to form granular iron formation. In addition to intraclasts, grainstone beds also contain sand-sized concentrically coated hematite grains (Fig. 4B, C; Facies F4, F5). Coatings are interpreted

to have precipitated just beneath the seafloor and thus, reflect variations in saturation state and Eh of pore water as well as the degree of sediment reworking (Akin et al., 2013; Pufahl et al., 2014). The ubiquitous presence of microcrystalline chert cement between grains indicates pore waters were silica saturated. Authigenic, isopachous greenalite rims around some grains indicate pore waters were also Fe-rich and became anoxic during burial (Fig. 4C; Facies F5; Klein, 2005). Euhedral, fabric destructive magnetite replaced grains and is the last phase to have precipitated (Fig. 4C; Facies F5) during burial diagenesis and low-grade metamorphism (prehnite-pumpellyite facies).

The anoxic paragenetic pathway is characterised by magnetite, chert, and greenalite that precipitated in coastal areas away from photosynthetic oxygen oases or in deeper anoxic regions of the shelf below the oxygen chemocline (Pufahl et al., 2014). The conversion of Fe-(oxyhydr)oxide to magnetite likely occurred through the addition of ferrous Fe via diffusion from the overlying anoxic water column or bacterial dissimilatory iron reduction (Raiswell, 2006; Johnson et al., 2008). In laminated iron formation, this authigenic magnetite was later recrystallised to late-stage, fabric destructive magnetite that overprints a mixture of microcrystalline chert and greenalite (Fig. 4D, E; Facies F6, F7). Anoxic grainstones contain abundant, sand-sized intraclasts of subhedral, fabric retentive magnetite that is commonly replaced by chert and greenalite (Fig. 4F; Facies F6). As in suboxic facies, textural relations indicate greenalite is authigenic and precipitated from low Eh pore water enriched in ferrous Fe and silica. Microcrystalline chert forming laminae and cementing grains also reflects the progressive diagenetic conversion of opal-A to quartz (Maliva et al., 2005).

5.2. Whole rock geochemistry

The major and trace element concentrations of 33 whole-rock samples from the Sokoman Formation indicate that the major component is Fe followed by lesser amounts of Mg, Ca, Mn, Al, P and Ti (Tables S1 and S2). The Fe and Mn serve as partial hydrothermal proxies whereas Al and Ti are direct proxies for clastic input. Absence of correlation between Ti and Al from various depths of the core, low absolute concentrations of Al and Ti (Fig. 5a) and extremely low concentrations of incompatible elements such as Th (< 0.03 ppm), Hf (< 0.04 ppm), Sc (< 0.03 ppm) and Zr (< 2 ppm) reflect a non-detrital origin for the silicates (Mloszewska et al., 2012). The Zn/Co ratio is the tracer of hydrothermal input (Toth, 1980) and high values for most of the

samples from various depths of the core are consistent with trace metals derived from a largely hydrothermal source. However, lack of correlation between δ^{57}Fe, Zn/Co ratios and water depth (Fig. 5b) is consistent with hydrothermal Fe carried from the hydrothermal source, likely by upwelling.

MORB normalized REE patterns for the whole-rock samples are shown in Fig.6 (a-d). Samples were normalized to MORB to compare against true hydrothermal values. Yttrium and REE are discussed together as these elements are geochemically similar. Iron formations contain low REE concentrations with $(Pr/Yb)_{MORB}$ values of 1.43-4.90, indicating light REE (LREE) enrichment and relative heavy REE (HREE) depletion for all samples. Europium anomalies were calculated using $Eu/Eu^* = Eu_{MORB}/ (0.66Sm_{MORB} + 0.33\ Tb_{MORB})$, which is a slightly modified version of the usual method of calculating these anomalies as seawater has a slight Gd anomaly (Li et al., 2013). A Ce/Ce* and Pr/Pr* diagram (Bau and Dulski, 1996) was used to determine Ce anomaly values using $Ce/Ce^* = Ce_{MORB}/ (0.5\ Pr_{MORB} + 0.5\ La_{MORB})$ and $Pr/Pr^* = Pr_{MORB}/ (0.5Ce_{MORB} + 0.5\ Nd_{MORB})$. Most of the Sokoman Iron Formation samples show positive Ce_{MORB} anomalies (Fig. 7a) and slightly positive Eu anomalies with Eu/Eu* values of 1.01-2.02 (Fig. 7b), although few samples record both negative Ce_{MORB} and Eu anomalies (Fig 7a and 7b). Lack of co-variations of Zr with Y/Ho and Y/Ho with Ce/Ce* indicate minimal crustal influences.

5.3. Oxygen isotopic composition of quartz and magnetite

The O isotopic compositions of quartz and magnetite separates from 14 whole rock samples are shown in Table 1 and Figure 8. The quartz separates have δ^{18}O values ranging from 17.1‰ to 23.9‰, averaging 19.7‰. The magnetite separates have δ^{18}O values ranging from -2.4‰ to 3‰ with an average of 0.6‰. The oxygen isotopic composition of magnetite and quartz were analyzed to understand the interaction of these minerals with diagenetic or metamorphic fluids and hence to interpret the effect of very low-grade metamorphism on O isotope variability. Li et al., (2013), concluded from the study of Dales Gorge Iron Formation that quartz and magnetite with high δ^{18}O values indicate isotopic exchange between minerals and fluids at elevated temperatures during post depositional process whereas magnetite with the lowest δ^{18}O value represents the most primitive magnetite. Differences between the δ^{18}O values of quartz and magnetite in the Sokoman samples have apparent isotopic equilibrium temperatures from 145°C

to 310°C (Figure 8), which may record fluid-rock interactions with fluids having high $\delta^{18}O$ values near 8‰ at these temperatures.

5.4. Fe isotopic composition

The Fe isotopic composition of 31 whole rock samples and 21 magnetite separates are shown in Table 2 and Figure 9. The general $\delta^{56}Fe$ trend for the bulk samples is a progressive decrease through each of the two depositional sequences, with an increase in values part way through sequence 2 (Fig. 9). The $\delta^{56}Fe$ values decrease from 0.47‰ to -0.35‰ and from -0.29‰ to -0.32‰ through the first and second sequences, respectively. This trend tracks the stacking of offshore over nearshore lithofacies as relative sea level rose. This trend is repeated as similar lowstand, transgressive, and highstand deposits are stacked during the accumulation of the second sequence.

Iron isotopic compositions of 21 magnetites exhibit the same trend, but the values are higher than the whole rock data. This difference is interpreted to reflect the presence of other Fe-mineral in whole rock samples whose $\delta^{56}Fe$ values are lower than those of the magnetites. The $\delta^{56}Fe$ values decrease from 0.10‰ to -0.29‰ and from -0.19‰ to -0.21‰ through the first and second sequences, respectively.

6. Discussion

6.1. REE patterns in Fe formation as tracers of ancient redox ocean

Alteration does not significantly modify REE contents in iron formation (Derry and Jacobsen, 1990) and thus coupling stratigraphy, REE compositions and other geochemical proxies can help constrain ocean redox conditions (e.g. Derry and Jacobsen, 1990). Fe oxides essentially record the REE patterns of the waters from which they precipitated and therefore act as paleoenvironmental proxies. The oxidation of Fe^{2+} to Fe^{3+} and subsequent precipitation from seawater occurs in the oxidation-reduction transition zone. In a stratified basin with oxidizing surface waters, metal oxides such as Mn (IV) oxyhydroxides adsorb Ho, LREE and Ce^{4+} in contrast to Fe(III) hydroxides that have low Ce, LREE and Ho concentrations (Bau, 1999; De Carlo et al., 2000;Ohta and Kawabe, 2001). In an anoxic water column, subsequent reductive

dissolution of these Mn oxides increases the Ce^{4+}, Ho and LREE concentrations in these waters. Precipitation of Fe-(oxyhydr)oxide from these anoxic waters result in positive Ce anomalies that persist through low grade metamorphism (Bau and Dulski, 1996; Slack et al., 2007). This leads to iron formations with positive Ce anomalies (Fig. 7), low Y/Ho and high LREE/HREE ratios (de Baar et al., 1988; Schijf et al., 1995; Bau et al., 1997b; De Carlo and Green, 2002; Pufahl and Hiatt, 2012).

The significant range of LREE/HREE (Fig. 6) and Y/Ho ratios in the Sokoman Iron Formation facies implies varying contributions of REE+Y from dissolution and precipitation of Mn-Fe (oxyhydr)oxides and their deposition under varying redox conditions in a basin with a strong chemocline separating the suboxic to anoxic deeper portion from the oxic upper portion of the water column (Planavsky et al., 2009; Bekker et al., 2010; Pufahl, 2010; Pufahl and Hiatt, 2012). Modest negative Ce anomalies for 4 samples of shallow water facies F2 and F3 ($Ce/Ce^* = 0.53$-0.77, accompanied by $Pr/Pr^* > 1$) indicate that their formation occurred in association with surface waters sufficiently oxic to scavenge Ce, similar to oxic and suboxic water masses of modern oceans (Elderfield and Greaves, 1982; Klein, 2005, Ohta and Kawabe, 2001; Piper et al, 1988; Planavsky et al., 2010). Samples with positive Eu anomalies (Fig. 7) indicate precipitation from waters influenced by submarine hydrothermal fluids (Danielson et al., 1992, Bau and Dulski, 1996). These fluids, however, generally have elevated Cu, Co, Ni concentrations (Klein and Ladeira, 2000), which contrast with the low concentrations in iron formation of the Sokoman Formation. Such low concentrations of these metals from various depths of core HR1279D support sedimentologic data that indicate iron formation was from a water column with periodic upwelling of Fe carried far from its hydrothermal source and from which these metals were scavenged. Similarly, samples with negligible Eu anomalies from various depths of the core HR1279D indicate that they do not represent proximal hydrothermal deposits but were probably generated by relatively cool hydrothermal solutions at some distance from their source vents.

6.2. Oxygen isotope of magnetite and quartz defining fluid-rock interaction

Concentrations of oxygen in quartz, magnetite and water are 53 wt‰, 27 wt‰ and 89 wt%, respectively, so that any alteration of the original $\delta^{18}O$ values of both quartz and magnetite either requires closed system exchange of oxygen between the minerals or high water/rock ratios

during metamorphism. If quartz and magnetite were originally precipitated in near equilibrium at 25°C with seawater having a $\delta^{18}O$ value 0‰, their $\delta^{18}O$ values would be near +33 and -6 (Fig. 8), respectively. The values we obtain, independent of modal abundance of magnetites, are far lower for quartz and far higher for magnetite (Fig. 8), and consistent with "apparent" oxygen isotope equilibration temperatures of 140 - 310°C. The relationship between the $\delta^{18}O$ values of coexisting magnetite and quartz do not record a steep fluid buffered disequilibrium array indicating open-system exchange as shown by Gregory et al. (1989). Rather, they plot between, and parallel, isothermal equilibration lines corresponding to 150°C and 350°C. If fluid absent closed system conditions prevailed during diagenesis, the $\delta^{18}O$ value of magnetite would change in proportion to the modal abundance of magnetite (Gregory et al., 1989), resulting in a vertical array of data points if quartz has a high modal abundance as in quartz-rich layers or a horizontal array if the modal abundance of quartz were low. There is random variation of the modal abundance of magnetites in our samples that plot along the equilibration lines, indicating oxygen isotope exchange occurred among fluid, magnetite and quartz at low temperatures. However, the mineral pair corresponding to the highest temperature (~310°C) and the lowest temperature (~140°C) is from adjacent locations, at depths of 31 m and 40 m of drill core HR1279D, respectively. Thus, the calculated apparent isotope equilibration temperatures between coexisting quartz-magnetite pairs can only be used to estimate the range of possible temperatures. Using the techniques described by Gregory et al. (1989) for evaluating open system exchange, it is unclear which mineral was most affected, suggesting that the system was more closed and rock-dominated during recrystallization of quartz and magnetite. The calculated high $\delta^{18}O$ values of the fluids near +8‰ are also expected in a rock-dominated, closed system.

6.3. Facies related Fe isotope variability in a well-constrained stratigraphic framework

The lack of correlation between metamorphic grade and calculated bulk $\delta^{56}Fe$ values of the Paleoproterozoic Biwabik Iron Formation from the Lake Superior region of North America also suggests that the original isotopic signature can be preserved during alteration (Frost et al., 2007; Hyslope et al., 2008; Li et al., 2013). The Fe isotopic data presented herein provide further evidence that in spite of prehnite-pumpellyite metamorphism, the primary Fe isotopic composition of iron formation lithofacies can be preserved. When these data are considered in an integrated paleoenvironmental, sequence stratigraphic, and paragenetic context, the relationship

between δ^{56}Fe values and sea level is compelling (Fig. 9). The decreasing trend in whole rock and magnetite δ^{56}Fe values through each sequence in the Sokoman Formation suggests that the isotopic composition was not appreciably influenced by authigenic microbial fractionations of Fe (Johnson et al. 2004). Instead, the stratigraphic variability in δ^{56}Fe values is more consistent with stacking of diachronous lithofacies through changing sea level regardless of the Fe-bearing minerals that precipitated.

In a marine stratified basin, Fe^{2+}_{aq} from upwelling of hydrothermal sources is oxidized to Fe^{3+}_{solid} and ultimately deposited as Fe-(oxyhydr)oxide below the chemocline/redoxcline in the lower anoxic layer through a number of abiotic and biotic processes (Klein, 2005; Johnson et al., 2008; Bekker et al., 2010; Pufahl, 2010; Pufahl and Hiatt, 2012). An important abiotic pathway for magnetite (mag) precipitation involves the settling of $Fe(OH)_3$ into Fe^{2+}_{aq}- rich anoxic bottom waters, followed by addition of Fe^{2+} of seawater to $Fe(OH)_3$ to form magnetite (Johnson et al., 2008).

$$Fe^{2+}_{aq} \xrightarrow[pathway1,\ in\ oxic\ layer]{oxidation} Fe(OH)_3 \xrightarrow[pathway\ 2,\ in\ anoxic\ layer]{precipitation} Fe(OH)_3 \xrightarrow[pathway\ 3,\ in\ anoxic\ layer]{Fe^{2+}_{aq}} \text{Magnetite...(1)}$$

Oxidation of Fe^{2+}_{aq} to $Fe(OH)_3$ (pathway 1) produces nearly 1.5‰ ^{56}Fe enrichment in $Fe(OH)_3$ with respect to the Fe^{2+}_{aq} ($\Delta^{56}Fe_{Fe(OH)3-\ Fe^{2+}aq}$ = 1.5‰; Johnson et al., 2008). Precipitation of Fe^{3+} as $Fe(OH)_3$ (pathway 2) results in minimal fractionation of Fe isotopes (Skulan et al, 2002; Dauphas and Rouxel, 2006). The Fe isotope composition of magnetite formed by pathway 3 of equation 1 reflects simple addition of Fe^{3+} and Fe^{2+} sources and therefore, $\delta^{56}Fe_{magnetite}$ values will be determined by the equation:

$\delta^{56}Fe^{2+}_{aq}$* (fraction of Fe^{2+}_{aq} in mag) + δ^{56} $Fe(OH)_3$* (fraction of $Fe(OH)_3$ in mag) = $\delta^{56}Fe_{mag}$.....(2)

The stoichiometric proportion of Fe^{2+} and Fe^{3+} to form magnetite through pathway 3 of equation 1 is well constrained at a ratio of 1:2. We assume $\delta^{56}Fe^{2+}_{aq}$ of -0.5‰ for seawater, which is an average of reported $\delta^{56}Fe^{2+}_{aq}$ values ranging between -0.1 and -0.8‰ (Johnson et al., 2008). Therefore, the variation of $\delta^{56}{}_{mag}$ will be controlled by the variation of δ^{56} $Fe(OH)_3$. We

consider two end member conditions, equilibrium and kinetic iron isotopic fractionation, for the formation of $Fe(OH)_3$ from oxidation of Fe^{2+}_{aq}. In case of equilibrium iron isotope fractionation between $Fe(OH)_3$ and Fe^{2+}_{aq} (pathway 1), the δ^{56} value of $Fe(OH)_3$ will be 1‰ and considering Fe^{2+}_{aq} of -0.5‰ the magnetite formed from this $Fe(OH)_3$ will have a value of 0.5‰. In the case of kinetic isotopic fractionation, where rapid precipitation does not allow isotopic equilibrium between Fe^{2+}_{aq} and $Fe(OH)_3$, the δ^{56} value of $Fe(OH)_3$ will be very close to δ^{56} value of Fe^{2+}_{aq} (-0.5‰). Similarly, if Fe^{2+}_{aq} completely converts to $Fe(OH)_3$, the δ^{56} of $Fe(OH)_3$ will be analogous to that value of Fe^{2+}_{aq} and the magnetite formed from this $Fe(OH)_3$ will have a value of -0.5‰. The $\delta^{56}Fe_{mag}$ values in this study range between -0.29 and +0.22‰ suggesting a combination of these two end member processes for the formation of magnetite.

Another pathway for the formation of magnetite at or below the sediment-water interface is the reaction between precipitated $Fe(OH)_3$ and Fe^{2+}_{aq} produced by dissimilatory iron reduction process (DIR, Johnson et al., 2005; 2008). This process produces a 3‰ ^{56}Fe depletion in Fe^{2+}_{aq} with respect to $Fe(OH)_3$ ($\Delta^{56}Fe_{Fe^{2+}aq - Fe(OH)3}$ = -3‰; Johnson et al., 2008) and magnetite produced from that Fe^{2+}_{aq} results in 1.3‰ higher $\delta^{56}Fe$ value than the value of Fe^{2+}_{aq} ($\Delta^{56}Fe_{mag}$ - $_{Fe^{2+}aq}$ = 1.3‰, Johnson et al., 2008). Therefore, magnetite formed through the DIR process yields a $\delta^{56}Fe$ value of -0.7‰ if the $\delta^{56}Fe$ value of precursor $Fe(OH)_3$ is 1‰. This process cannot explain the range of $\delta^{56}Fe_{mag}$ in this study. Furthermore, direct precipitation of magnetite from Fe^{2+}_{aq} of seawater yields a $\delta^{56}Fe_{mag}$ value of 1.06‰ considering the equilibrium $\Delta^{56}Fe_{mag}$ - $_{Fe^{2+}aq}$ = 1.56‰ at 22°C (Frierdich et al., 2014). Such high $\delta^{56}Fe_{mag}$ values were not observed in this study indicating that direct precipitation of magnetite from Fe^{2+}_{aq} is not the pathway for magnetite formation.

In shallow paleoenvironments of the Sokoman Formation, seawater and photosynthetic oxygen were mixed by waves to produce an unstratified, suboxic water column (Pufahl et al., 2014) that was somewhat removed from circulation with the open ocean because of its coastal nature. Thus, the higher $\delta^{56}Fe$ values that characterize shallow lithofacies are interpreted to record precipitation from a seawater reservoir that was slow to recharge with the open ocean. Consequently, there was sufficient time to reach isotopic equilibrium between Fe^{2+}_{aq} and precipitating $Fe(OH)_3$ to produce magnetite with a $\delta^{56}Fe$ value of 0.5‰.

As transgression ensued and water depth rose, progressively deeper water lithofacies accumulated beneath a well-stratified water column with a prominent oxygen chemocline (Pufahl et al., 2014). Seawater that bathed the middle shelf was constantly recharged through upwelling, which provided a sustained supply of Fe^{2+}_{aq} to mix with dissolved oxygen and precipitate $Fe(OH)_3$ (Fig. 10). Although the delivery of Fe^{2+}_{aq} to the surface ocean was relatively constant, precipitation was rapid resulting in short residence times (ca. 1.5 to 45 years; Hodell et al., 1989; Berner and Berner, 1996; Johnson et al., 2003) and very low Fe^{2+}_{aq} concentrations (ca. 50 ppt; Rue and Bruland, 1995). Such rapid reaction rates would have precluded equilibrium precipitation of $Fe(OH)_3$.

Because precipitation was much slower in the anoxic seawater beneath, residence times were exceedingly long (ca. 1.5 million years; Johnson et al., 2003) and concentrations of Fe^{2+}_{aq} were orders of magnitude higher (ca. 50 ppm; Ewers, 1983; Summer, 1997). An anoxic deep ocean in the Paleoproterozoic permitted hydrothermal Fe to concentrate over millions of years, producing a seawater reservoir that was periodically tapped by upwelling (Pufahl and Hiatt, 2012; Pufahl et al., 2014). Kinetic isotopic fractionation between Fe^{2+}_{aq} and $Fe(OH)_3$ in these deeper anoxic waters (Fig. 10) forms magnetite with a $\delta^{56}Fe$ value close to -0.5‰.

Thus, the decreasing trend in δ^{56} Fe values through transgressive and highstand deposits of the Sokoman Formation are interpreted to record the precipitation of Fe from a water column that became progressively more open marine with time. Notably, values defining this trend are independent of the Fe-bearing mineral phase that precipitated. However, progressively lower $\delta^{56}Fe$ in the deep water facies are associated with siderite with a low $\delta^{56}Fe$ and is precipitated in more reducing, deeper, pore waters (Pufahl, 2010). Minute $\delta^{56}Fe$ variations in facies specific stratigraphic sections of the core probably correspond to several upwelling and fluctuations within a large-scale transgressive process.

7. **Conclusions**

1) Geochemical assessment of the Paleoproterozoic Sokoman Iron Formation, which consists of seven lithofacies, has been carried out to elucidate any connection to alteration, effect of low-grade metamorphism and depositional environment on Fe isotopic variability. Field and petrographic observations, mineral paragenesis and textural

relations reveal deposition of Fe in an upwelling marine transgressive and regressive environment. Extremely low concentrations of incompatible elements such as Th, Hf, Sc and Zr and absence of correlation between Ti and Al are consistent with a non-detrital origin for the silicates. Poor correlation between δ^{57}Fe and Zn/Co indicates that iron formation samples were deposited at some distance away from a hydrothermal source due to upwelling. All Sokoman samples exhibit LREE enrichment and in combination with slight positive Eu anomalies, or attenuated positive as well as negative Eu anomalies, indicate that the sediments derived dominantly from a low temperature hydrothermal source but deposited away from source vents due to mixing and upwelling. Most of the Sokoman Iron Formation samples show positive Ce_{MORB} anomalies, which is due to reductive dissolution of Mn oxides in anoxic and suboxic waters. However, very few samples show negative Ce_{MORB} anomalies because of their deposition close to the chemocline in oxic shallow water.

2) The δ^{18}O of quartz and magnetite pairs indicate that metamorphism of the Sokoman Formation reached apparent temperatures of 140 to 310°C. The calculated δ^{18}O values of fluids in apparent equilibrium with these minerals range from 5.7‰ to 11.4‰, consistent with relatively closed-system exchange and low fluid/rock ratios.
3) The Sokoman whole rock and magnetite δ^{56}Fe values indicate that at the beginning of marine transgression, partial oxidation of Fe^{2+}_{aq} and near isotopic equilibrium between Fe^{2+}_{aq} and $Fe(OH)_3$ lead to magnetite formation with positive δ^{56}Fe values because the available pool was not as readily recharged. In contrast, during marine transgression, Fe^{2+}_{aq} delivered to the oxygenated surface ocean through upwelling was converted to $Fe(OH)_3$ very rapidly. The kinetic isotopic fractionation between Fe^{2+}_{aq} and $Fe(OH)_3$ in deeper anoxic ocean water resulted in the precipitation of magnetite with lower δ^{56}Fe values in middle and distal shelf environments (Fig. 10).This Fe isotope variability as a function of sedimentary environment transcends the Fe minerals that precipitated in each facies. This shift from higher to lower δ^{56}Fe values is well documented in the stratigraphic section and thus provides insight into paleo-depositional conditions. A combination of kinetic and near equilibrium fractionation processes produced the range of δ^{56}Fe values (0.22 to -0.29‰) of magnetites in this study. Thus, in spite of low grade metamorphism and alteration recorded in the oxygen isotopes of paired quartz-

magnetite, a holistic study of drill core HR1279D from the Sokoman Formation implies that it still preserves the primary Fe isotopic patterns that reflect paleoenvironment and thus tracks sea level, including differences in the mixing rates of seawater and the Fe pool in nearshore versus offshore areas of the shelf. The Fe isotopic compositions and their variability do not really record the effects from microbial fractionations that occur when various Fe-bearing minerals precipitate.

8. Acknowledgements

This research was funded by the Canadian Natural Sciences and Engineering Research Council Discovery grants to T. Kurtis Kyser and Peir K. Pufahl. We wish to thank April Vuletich, Evelyne Leduc, Don Chipley, Brian Joy and Kristen Gault at the Queen's Facility for Isotope Research for technical support. We would like to thank three anonymous reviewers for their constructive reviews of this manuscript and Associate Editor Andrew Bowie for his assistance.

References

Akin S. J., Pufahl P. K., Hiatt E. E., and Pirajno F. (2013) Oxygenation of shallow marine environments and chemical sedimentation in Palaeoproterozoic peritidal settings: Frere Formation, Western Australia. *Sedimentology* **60**, 1599-1582.

Anderson S. L. (2009) The sedimentology of phosphatic iron formation from the Labrador Trough: implications for the accumulation of Precambrian phosphorite, M.Sc. Thesis, Department of Earth and Environmental Science, Acadia University, Wolfville, NS.

Balci N., Bullen T. D., Witte-Lien K., Shanks W. C., Motelica M., and Mandernack K. W. (2006) iron isotope fractionation during microbially stimulated Fe(II) oxidation and Fe(III) precipitation. *Geochimica et Cosmochimica Acta* **70**(3), 622-639.

Bau M. (1999) Scavenging of dissolved yttrium and rare earths by precipitating iron oxyhydroxide: experimental evidence for Ce oxidation, Y-Ho fractionation, and lanthanide tetrad effect. *Geochimica et Cosmochimica Acta* **63**(1), 67-77.

Bau M. and Dulski P. (1996) Distribution of yttrium and rare-earth elements in the Penge and Kuruman iron-formations, Transvaal Supergroup, South Africa. *Precambrian Research* **79**(1-2), 37-55.

Bau M., Möller P., and Dulski P. (1997) Yttrium and lanthanides in eastern Mediterranean seawater and their fractionation during redox-cycling. *Marine Chemistry***56**(1-2), 123-131.

Beard B. L., Johnson C. M., Damm K. L. V., and Poulson R. L. (2003) Iron isotope constraints on Fe cycling and mass balance in oxygenated Earth oceans. *Geology* **31**(7), 629-632.

Becker R. H. (1976) Oxygen isotope study of a Precambrian banded iron-formation, Hamersley Range, Western Australia. *Geochimica et Cosmochimica Acta* **40**(10), 1153-1165.

Bekker A., Slack J. F., Planavsky N., Krapež B., Hofmann A., Konhauser K. O., and Rouxel O. J. (2010) Iron Formation: The Sedimentary Product of a Complex Interplay among Mantle, Tectonic, Oceanic, and Biospheric Processes. *Economic Geology* **105**(3), 467-508.

Berner E. K. and Berner R. A. (1996) Global environment water air and geochemical cycles. *Prentice Hall, New Jersey*.

Borrok D. M., Wanty R. B., Ridley W. I., Wolf R., Lamothe P. J., and Adams M. (2007) Separation of copper, iron, and zinc from complex aqueous solutions for isotopic measurement. *Chemical Geology* **242**(3-4), 400-414.

Bullen T. D., White A. F., Childs C. W., Vivit D. V., and Schulz M. S. (2001) Demonstration of significant abiotic iron isotope fractionation in nature. *Geology* **29**(8), 699-702.

Catuneanu O., Abreu V., Bhattacharya J. P., Blum M. D., Dalrymple R. W., Eriksson P. G., Fielding C. R., Galloway W. E., Gibling M. R., Giles K. A., Holbrook J. M., Jordanm R., Kendalln C. G. S. C., Macurdao B., Martinsenp O. J., Miallq A. D., Nealb J. E., Nummedalr D., Pomars L., Posamentiert H. W., Prattu B. R., Sargv J. F., Shanleyw K. W., Steelh R. J., Strasserx A., Tuckery M. E., and Winkerz C. (2009) Towards the standardization of sequence stratigraphy. *Earth-Science Reviews* **92**(1-2), 1-33.

Chauvel J. and Dimroth E. (1974) Facies types and depositional environment of the Sokoman Iron Formation, central Labrador Trough, Quebec, Canada. *Journal of Sedimentary Petrology* **44**, 299-327.

Clark T. and Wares R. (2004) Syntheselitho tectoniqueet metallogenique de l'Orogene du Nouveau-Quebec (Fosse du Labrador).Ministere des Ressources naturelles, Quebec, (MM 2004-01).

Clark T. and Wares R. (2006) Lithotectonic and Metallogenic Synthesis of the New Quebec Orogen (Labrador Trough). *In: Choiniere, J. (Ed.) Ministere des Ressources naturelleset de la Faune, Quebec, MM 2005-01*.

Clayton R. N. and Mayeda T. K. (1963) The use of bromine pentafluoride in the extraction of oxygen from oxides and silicates for isotopic analysis. *Geochimica et Cosmochimica Acta* **27**, 43-52.

Cloud P. (1973) Paleoecological Significance of the Banded Iron-Formation. *Economic Geology* **68**(7), 1135-1143.

Clout J. M. and Simonson B. M. (2005) Precambrian iron formations and iron formation-hosted ore deposits. *Economic Geology*. Society of Economic Geologists, 100th Anniversary, 643-679.

Condie K. C., Marais D. J. D., and Abbott D. (2001) Precambrian superplumes and supercontinents: a record in black shales, carbon isotopes, and paleoclimates? *Precambrian Research* **106**, 239-260.

Croal L. R., Johnson C. M., Beard B. L., and Newman D. K. (2004) Iron isotope fractionation by Fe(II)-oxidizing photoautotrophic bacteria. *Geochimica et Cosmochimica Acta* **68**(6), 1227-1242.

Danielson A., Möller P., and Dulski P. (1992) The europium anomalies in banded iron formations and the thermal history of the oceanic crust. *Chemical Geology* **97**(1-2), 89-100.

Dauphas N., Cates N. L., Mojzsis S. J., and Busigny V. (2007) Identification of chemical sedimentary protoliths using iron isotopes in the >3750 Ma Nuvvuagittuq supracrustal belt, Canada. *Earth and Planetary Science Letters* **254**(3-4), 358-376.

Dauphas N. and Rouxel O. (2006) Mass spectrometry and natural variations of iron isotopes. *Mass Spectrometry Reviews* **25**(4), 515-550.

Dauphas N., Zuilen M. v., Wadhw M., Davis A. M., Marty B., and Janney P. E. (2004) Clues from Fe Isotope Variations on the Origin of Early Archean BIFs from Greenland. *Science* **306**(5704), 2077-2080.

deBaar H. J. W., German C. R., Elderfield H., and Gaans P. v. (1988) Rare earth element distributions in anoxic waters of the Cariaco Trench. *Geochimica et Cosmochimica Acta* **52**(5), 1203-1219.

DeCarlo E. H. and Green W. J. (2002) Rare earth elements in the water column of Lake Vanda, McMurdo Dry Valleys, Antarctica. *Geochimica et Cosmochimica Acta* **66**(8), 1323-1333.

DeCarlo E. H., Wen X.-Y., and Cowen J. P. (2000) Rare earth element fractionation in hydrogenetic Fe-Mn crusts: The influence of carbonate complexation and phosphatization on Sm/Yb ratios, C.R. Glenn, L. Prevot-Lucas, J. Lucas (Eds.), Marine Authigenesis: From Global to Microbial. *Society for Sedimentary Geology*. Special Volume **66**, 271–285.

Derry L. A. and Jacobsen S. B. (1990) The chemical evolution of Precambrian seawater: Evidence from REEs in banded iron formations. *Geochimica et Cosmochimica Acta* **54**, 2965-2977.

Dimroth E. and Dressler B. (1978) Metamorphism of the Labrador Trough. *Paper - Geological Survey of Canada 78-10*, 215-236.

Edwards C. T., Pufahl P. K., Hiatt E. E., and Kyser T. K. (2012) Paleoenvironmental and taphonomic controls on the occurence of Paleoproterozoic microbial communities in the 1.88 Ga Ferriman Group, Labrador Trough, Canada. *Precambrian Research* **212-213**, 91-106.

Elderfield H. and Greaves M. J. (1982) The rare earth elements in seawater. *Nature* **296**, 214-219.

Evans D. A. D. and Mitchell R. N. (2011) Assembly and breakup of the core of Paleoproterozoic-Mesoproterozoic supercontinent Nuna. *Geology* **39**, 443-446.

Ewers W. E. (1983) Chemical factors in the deposition and diagenesis of banded iron-formation. In: Trendal AF, Morris RC (eds), Iron formations: facts and problems. Elsevier, Amsterdam. 491-512.

Findlay J. M., Parrish R. R., Birkett T. C., and Watanabe D. H. (1995) U-Pb ages from the Nimish Formation and Montagnais glomeroporphyritic gabbro of the central New Quebec Orogen, Canada. *Canadian Journal of Earth Sciences* **32**, 1208-1220.

Frierdich A. J., Beard B. L., Scherer M. M., and Johnson C. M. (2014) Determination of the Fe(II)aq – magnetite equilibrium iron isotope fractionation factor using the three – isotope method and a multi – direction approach to equilibrium. *Earth and Planetary Science Letters* **391**, 77-86.

Frost C. D., Blanckenburg F. v., Schoenberg R., Frost B. R., and Swapp S. M. (2007) Preservation of Fe isotope heterogeneities during diagenesis and metamorphism of banded iron formation. *Contributions to Mineralogy and Petrology* **153**, 211-235.

Gregory R. T., Criss R. E., and Taylor H. P. Jr. (1989) Oxygen isotope exchange kinetics of mineral pairs in closed and open systems: Applications to problems of hydrothermal alteration of igneous rocks and Precambrian iron formations. *Chemical Geology* **75**, 1-42.

Gross G. A. (1968) Geology of iron depositd in Canada; volume 3, iron ranges of the Labrador geosyncline. *Economic geology report. Geological Survey of Canada*.

Gross G. A. (1980) A classification of iron formations based on depositional environment. *Canadian Mining* **18**, 215-222.

Gross G. A. (1983) Tectonic systems and the deposition of iron-formation. *Developments in Precambrian Geology* **7**, 63-79.

Gross G. A. and Zajac I. S. (1983) Iron-formation in fold belts marginal to the Ungava craton Elsevier.

Hodell D. A., Mueller P. A., McKenzie J. A., and Mead G. A. (1989) Strontium isotope stratigraphy and geochemistry of the late Neogene ocean. *Earth and Planetary Science Letters* **92**, 165-178.

Hoffman P. F. (1988) United plates of America, the birth of a craton; early Proterozoic assembly and growth of Laurensia. *Annual Review of Earth and Planetary Sciences* **16**, 543-603.

Hyslop E. V., Valley J. W., Johnson C. M., and Beard B. L. (2008) The effects of metamorphism on O and Fe isotope compositions in the Biwabik Iron Formation, northern Minnesota. *Contributions to Mineralogy and Petrology* **155**, 313-328.

Johnson C. M., Beard B. L., Beukes N. J., Klein C., and O'Leary J. M. (2003) Ancient geochemical cycling in the Earth as inferred from Fe isotope studies of banded iron formations from the Transvaal Craton. *Contributions to Mineralogy and Petrology* **144**(5), 523-547.

Johnson C. M. and Beard B. L. (2004) Isotopic constraints on Biogeochemical Cycling of Fe.*Reviews in Mineralogy and Geochemistry* **55**, 359-408.

Johnson C. M., Beard B. L., Klein C., Beukes N. J., and Roden E. E. (2008) Iron isotopes constrain biologic and abiologicprecesses in banded iron formation genesis. *Geochimica et Cosmochimica Acta* **72**(1), 151-169.

Johnson C. M., Beard B. L., and Roden E. E. (2008b) The iron isotope fingerprints of redox and biogeochemical cycling in modern and ancient Earth. *Ann. Rev. Earth Planet Sci* **36**, 457-493.

Johnson C. M., Roden E. E., Welch S. A., and Beard B. L. (2005) Experimental constraints on Fe isotope fractionation during magnetite and Fe carbonate formation coupled to dissimilatory hydrous ferric oxide reduction. *Geochimica et Cosmochimica Acta* **69**(4), 963-993.

Johnson C. M., Skulan J. L., Beard B. L., Sun H., Nealson K. H., and Braterman P. S. (2002) Isotopic fractionation between Fe(III) and Fe(II) in aqueous solutions. *Earth and Planetary Science Letters* **195**(1-2), 141-153.

Kholodov V. N. and Butuzova G. Y. (2004) Problems of siderite formation and iron ore epochs: communication 1. Types of siderite-bearing iron ore deposits. *Lithology and mineral resources* **39**, 389-411.

Klein C. (1978) Regional metamorphism of Proterozoic iron-formation, Labrador Trough, Canada. *American Mineralogist* **63**, 898-912.

Klein C. (2005) Some Precambrian banded iron formations (BIFs) from around the worlds: Their age, geologic setting, mineralogy, metamorphism, geochemistry, and origins. *American Mineralogist* **90**(10), 1473-1499.

Klein C. and Fink R. P. (1976) Petrology of the Sokoman Iron Formation in the Howells River area, at the western edge of the Labrador trough. *Economic Geology* **71**, 453-487.

Klein C. and Ladeira E. A. (2000) Geochemistry and petrology of some Proterozoic banded iron formations of the Quadrilatero Ferrifero, Minas Gerais, Brazil. *Economic Geology* **95**, 405-428.

LaBerge G. L. (1964) Development of magnetite in iron formations of the Lake Superior region. *Geology* **59**, 1313-1342.

Li W., Huberty J.M., Beard B.L., Kita N.T., Valley J. W., and Johnson C.M. (2013) Contrasting behaviour of oxygen and iron isotopes in banded iron formations revealed by in situ isotope analysis. *Earth and Planetary Science Letters* **384**, 132-143.

Li Z., Zhu X., and Tang S. (2012) Fe isotope compositions of banded iron formation from Anshan-Benxi area: Constraints on the formation mechanism and Archean ocean environment. *Acta Petrologica Sinica* **28**, 3545-3558 (in Chinese with English abstract).

Machado N., Clark T., David J., and Goulet N. (1997) U-Pb ages for magmatism and deformation in the New Quebec orogen *Canadian Journal of Earth Sciences* **34**, 716-723.

Maliva R. G., Knoll A. H., and Simonson B. M. (2005) Secular change in the Precambrian silica cycle: Insights from chert petrology. *Bulletin of The Geological Society of America* **117**, 835-845.

Meert J. G. (2012) What's in a name? The Columbia (Paleopangaea/Nuna) supercontinent. *Gondwana Research* **21**, 987-993.

MloszewskaA. M., Pecoits E., Cates N. L., MojzsisS. J., O'Neil J., Robbins L. J., and KonhauserK.O. (2012) The composition of Earth's oldest iron formations: The NuvvuagittuqSupracrustal Belt (Québec, Canada). *Earth and Planetary Science Letters* **317-318**, 331-342.

Ohta A. and Kawabe I. (2001) REE(III) adsorption onto Mn dioxide (δ-MnO2) and Fe oxyhydroxide: Ce(III) oxidation by δ-MnO2. *Geochimica et Cosmochimica Acta* **65**(5), 695-703.

Piper D. Z., Baedecker P. A., Crock J. G., Burnett W. C., and Loebner B. J. (1988) Rare earth elements in the phosphatic-enriched sediment of the Peru Shelf. *Marine Geology* **80**, 269-285.

Planavsky N., Bekker A., Rouxel O. J., Kamber B., Hofmann A., Knudsen A., and Lyons T. W. (2010) Rare Earth Element and yttrium compositions of Archean and Paleoproterozoic Fe formations revisited: New perspectives on the significance and mechanisms of deposition. *Geochimica et Cosmochimica Acta* **74**(22), 6387-6405.

Planavsky N., Rouxel O., Bekker A., Shapiro R., Fralick P., and Knudsen A. (2009) Iron-oxidizing microbial ecosystems thrived in late Paleoproterozoic redox-stratified oceans. *Earth and Planetary Science Letters* **286**(1-2), 230-242.

Pufahl P. K. (2010) Bioelemental sediments, N.P. James, R.W. Dalrymple (Eds). *Facies Models. Geological Association of Canada, Canada*, 477-504.

Pufahl P. K., Anderson S. L., and Hiatt E. E. (2014) Dynamic sedimentation of Paleoproterozoic continental margin iron formation, Labrador Trough, Canada: paleoenvironments and sequence stratigraphy. *Sedimentary Geology* **309**, 48-65.

Pufahl P. K. and Fralick P. W. (2004) Depositional controls on Paleoproterozoic iron formation accumulation, Gogebic Range, Lake Superior region, USA. *Sedimentology* **51**, 791-808.

Pufahl P. K. and Hiatt E. E. (2012) Oxygenation of the Earth's atmosphere-ocean system: a review of physical and chemical sedimentologic responses. *Marine and Petroleum Geology* **32**, 1-20.

Raiswell R. (2006) An evaluation of diagenetic recycling as a source of iron for banded iron formations. In: Kesler, S.E., Ohmoto, H. (Eds.). *Geological Society of America, Boulder, Colorado,* 223-238.

Reddy S. M. and Evans D. A. D. (2009) Palaeoproterozoic supercontinents and global evolution: correlations from core to atmosphere. In: Reddy, S.M., Mazumder, R., Evans, D.A.D.,

Collins, A.S. (Eds.), Paleoproterozoic Supercontinents and Global Evolution. *Geological Society, London, Special Publications* **323**, 1-26.

Rue E. L. and Bruland K. W. (1995) Complexation of iron(III) by natural organic ligands in the Central North Pacific as determined by a new competitive ligand equilibration/adsorptive cathodic stripping voltammetric method. *Mar Chem* **50**, 117-138.

Schijf J., Baar H. J. W. D., and Millero F. J. (1995) Vertical distributions and speciation of dissolved rare earth elements in the anoxic brines of Bannock Basin, eastern Mediterranean Sea. *Geochimica et Cosmochimica Acta* **59**(16), 3285-3299.

Sheppard S. M. (1986) Characterization and isotopic variations in natural waters. *Reviews in Mineralogy and Geochemistry* **16**, 165-183.

Simonson B. M. (1984) High energy shelf-deposit; early Proterozoic Wishart Formation, northeastern Canada. *Special Publication - Society of Economic Paleontologists and Mineralogists* **34**, 251-268.

Simonson B. M. (2003) Origin and evolution of large Precambrian iron formations. *Special paper - Geological Society of America* **370**, 231-244.

Skulan J. L., Beard B. L., and Johnson C. M. (2002) Kinetic and equilibrium Fe isotope fractionation between aqueous Fe(III) and hematite. *Geochimica et Cosmochimica Acta* **66**(17), 2995-3015.

Slack J. F., Grenne T., Bekker A., Rouxel O. J., and Lindberg P. A. (2007) Suboxic deep seawater in the late Paleoproterozoic: Evidence from hematitic chert and iron formation related to seafloor-hydrothermal sulfide deposits, central Arizona, USA. *Earth and Planetary Science Letters* **255** (1–2), 243–256.

Steinhoefel G., Blanckenburg F. v., Horn I., Konhauser K. O., Beukes N. J., and Gutzmer J. (2010) Deciphering formation processes of banded iron formations from the Transvaal and the Hamersley successions by combined Si and Fe isotope analysis using UV femto second laser ablation. *Geochimica et Cosmochimica Acta* **74**(9), 2677-2696.

Summer D. Y. (1997) Carbonate precipitation and oxygen stratification in Late Archean seawater as deduced from facies and stratigraphy of the Gamohaan and Frisco

Formations, Transvaal Supergroup, South Africa. *American Journal of Science* **297**, 455-487.

Taylor P. D. P., Maeck R., and Bièvre P. D. (1992) Determination of the absolute isotopic composition and Atomic Weight of a reference sample of natural iron. *International Journal of Mass Spectrometry and Ion Processes* **121**(1-2), 111-125.

Toth J. R. (1980) Deposition of submarine crusts rich in manganese and iron.*GSA Bulletin* **91**(1), 44-54.

Trendall A. F. (2002) The significance of iron formation in the Precambrian stratigraphic record *Special publication of the International Association of Sedimentologists* **33**, 33-66.

Trendall A. F. and Blockley J. G. (2004) Precambrian iron formation. *Developments in Precambrian Geology* **12**, 403-421.

Wardle R. J. and Bailey D. G. (1981) Early Proterozoic sequences in Labrador. *Paper - Geological Survey of Canada 81-10*, 331-358.

Wardle R. J., James D. T., Scott D. J., and Hall J. (2002) The southeastern Churchill Province; synthesis of a Paleoproterozoic transpressional orogen. *Canadian Journal of Earth Sciences***39**, 639-663.

Welch S. A., Beard B. L., Johnson C. M., and Braterman P. S. (2002) Kinetic and equilibrium Fe isotope fractionation between aqueous Fe(II) and Fe(III). *Geochimica et Cosmochimica Acta* **67**(22), 4231-4250.

Zajac I. S. (1974) The stratigraphy and mineralogy of the Sokoman Formation in the Knob Lane Area, Quebec and Newfoundland. *Geological Survey of Canada Bulletin 220*, page 159.

Figure 1. A) Location and general geologic map of Schefferville area with location of drill core no. HR1279D along with other drill core locations; B) Stratigraphic cycles of the Labrador Trough and Ferriman Group. Modified from Clark and Wares (2006).

Figure 2. Stratigraphic section of the Ferriman Group from drill core HR1279 showing stacking of lithofacies (F1-F7) and mineralogical changes in the Ruth and Sokoman formations. Sea-level curve in upper right shows system tracts. SB = sequence boundary, LST= lowstand systems tract,

TST = transgressive systems tract, HST = highstand systems tract. Sequence stratigraphic nomenclature after Anderson, 2009 and Edwards, 2012.

Figure 3. Mineral paragenesis of iron formations in the Sokoman Formation for both anoxic and suboxic pathways.

Figure 4. A) Stromatolite-bearing flaser-bedded chert grainstone. Hematite (Hem; light grey crystals) and microcrystalline chert-rich (dark grey) mudstone (F3). Plane-polarized reflected light. B) Cross-stratified hematitic grainstone. Concentrically coated grains of mosaic hematite are cemented by microcrystalline quartz (Qtz) (F4). Cross-polarized transmitted and reflected light, polarizer 10º. C) Stromatolite-bearing flaser-bedded chert grainstone. Concentrically coated hematite grain (light grey) with acicular isopachous rim of greenalite (Gn). Fabric destructive magnetite (Mag2) (dark grey) overprints hematite, greenalite, and microcrystalline chert cement is between grains (F5). Plane-polarized transmitted and reflected light. D) Wavy- and cross-stratified magnetite-rich packstone. Laminae between packstones are formed of fabric destructive, euhedral magnetite (light grey) that overprints microcrystalline chert (F6). Plane-polarized transmitted and reflected light. E) Parallel-bedded, magnetite-rich chert grainstone. Fabric destructive magnetite (black) overprints greenalite and microcrystalline chert in laminae between grainy beds (F7). Cross-polarized transmitted light. F) Wavy- and cross-bedded magnetite-rich packstone. Chert and greenalite-replaced, sand-sized magnetite (Mag1) grain (black). Greenalite forms acicular aggregates within microcrystalline chert (F6). Cross-polarized transmitted light.

Figure 5. A) Bivariate plot showing lack of correlation between Ti (ppm) and Al (ppm) from various depths of core HR1279D, consistent with a non-detrital origin of silicates; B) Lack of correlation between δ^{57}Fe and Zn/Co from various depths of core HR1279D indicating remoteness of the samples from a hydrothermal source. Mineral assemblages from shallow depth, intermediate depth and greater depth are represented by filled circles, squares, and diamonds/ triangles respectively. Hem = hematite, Mag = magnetite, Cb = carbonate and Sil = silicate. Data from Table S1.

Figure 6. A-D) MORB normalized trace element patterns of Sokoman iron formation samples. All patterns record enrichment of LREE relative to HREE. Data from Table S2.

Figure 7. Relationship between Ce/Ce* and Pr/Pr*. Positive Ce anomalies for most iron formation samples are attributed to reductive dissolution in anoxic and suboxic waters whereas negative Ce anomalies from shallow water facies F2 and F3 reflect formation from oxic surface waters close to the chemocline; B) Relationship between Eu/Eu^*_{MORB} vs. Eu/Eu^*_{PAAS}. A combination of slight positive Eu anomalies, attenuated positive as well as negative Eu anomalies indicating sediments derived dominantly from a low temperature hydrothermal source but deposited away from source vents due to mixing and upwelling. Data from Table S2.

Figure 8. Relationship between $\delta^{18}O$ magnetite (mag) and $\delta^{18}O$ quartz (qtz). Lines indicate equilibrium values expected at 150°C, 250°C and 350°C. Modal abundance of magnetites is labelled in the figure. Apparent equilibrium temperature and corresponding $\delta^{18}O$ fluid composition are shown in Table 1.

Figure 9. Relationship between $\delta^{56}Fe$ values and stratigraphic position for whole rock samples (solid symbols) and magnetites (open symbols) for the Sokoman Formation. The $\delta^{56}Fe$ values are higher at the beginning of deposition and become progressively lower in each sequence. Data from Table 2.

Figure 10. Idealized depiction of a redox stratified basin consisting of an upper oxic and lower anoxic zone separated by a chemocline. Fe concentration in oxic layer is 50 ppt (Rue and Bruland, 1995), which is negligible compared to Fe concentration in anoxic layer which is 50 ppm (Ewers, 1983; Summer, 1997). Residence time of Fe^{2+}_{aq} in anoxic water is greater (~1.5million years) than residence time of Fe in oxic (< 45 years) water so that with progressive marine transgression and Fe^{2+}_{aq} influx in oxic layer from ocean upwelling, rapid precipitation of $Fe(OH)_3$ results in kinetic isotopic fractionation in contrast to sluggish coastal marine water where Fe^{2+}_{aq} and $Fe(OH)_3$ precipitate remains in near isotopic equilibrium.

Figure 1

A) B)

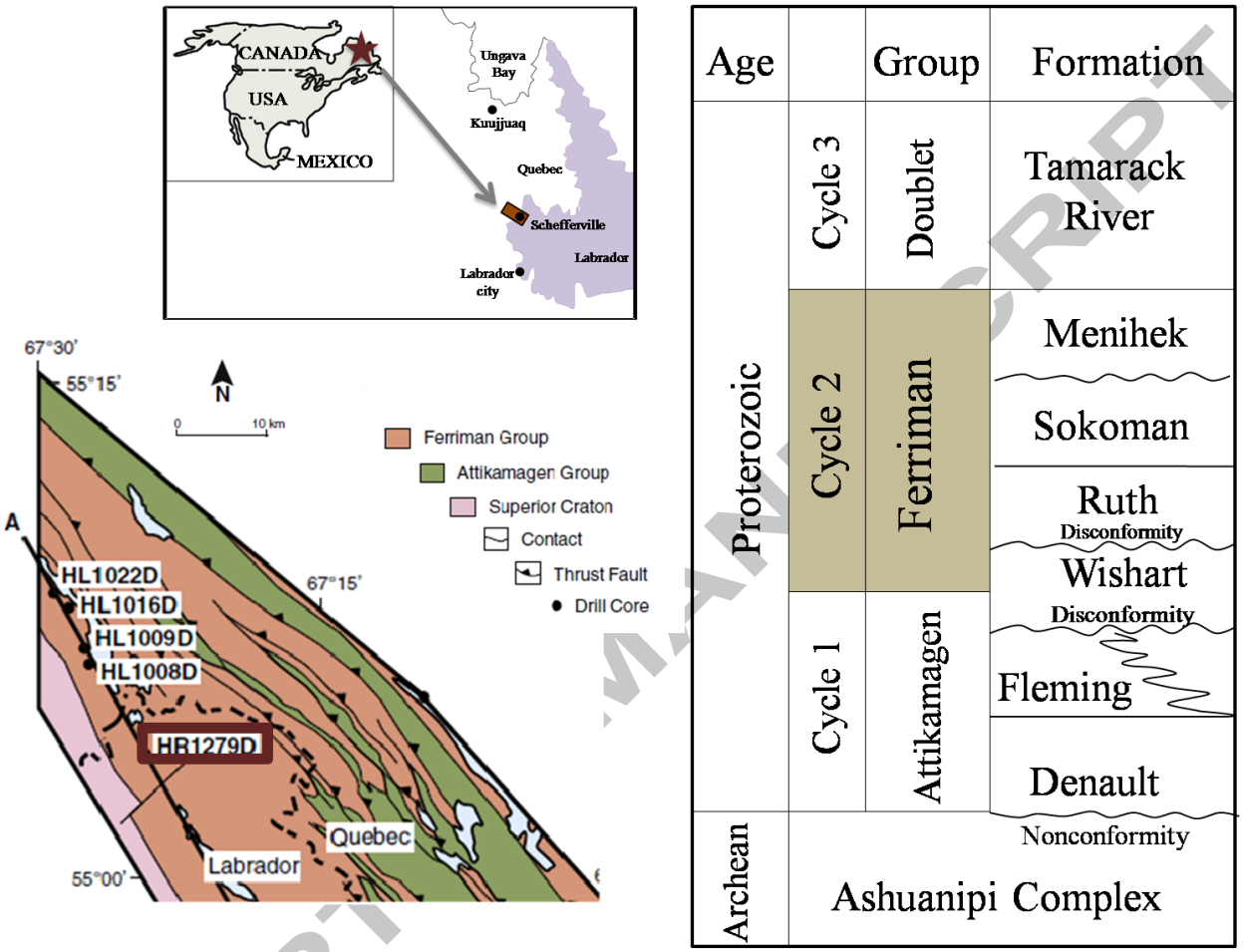

Figure 2

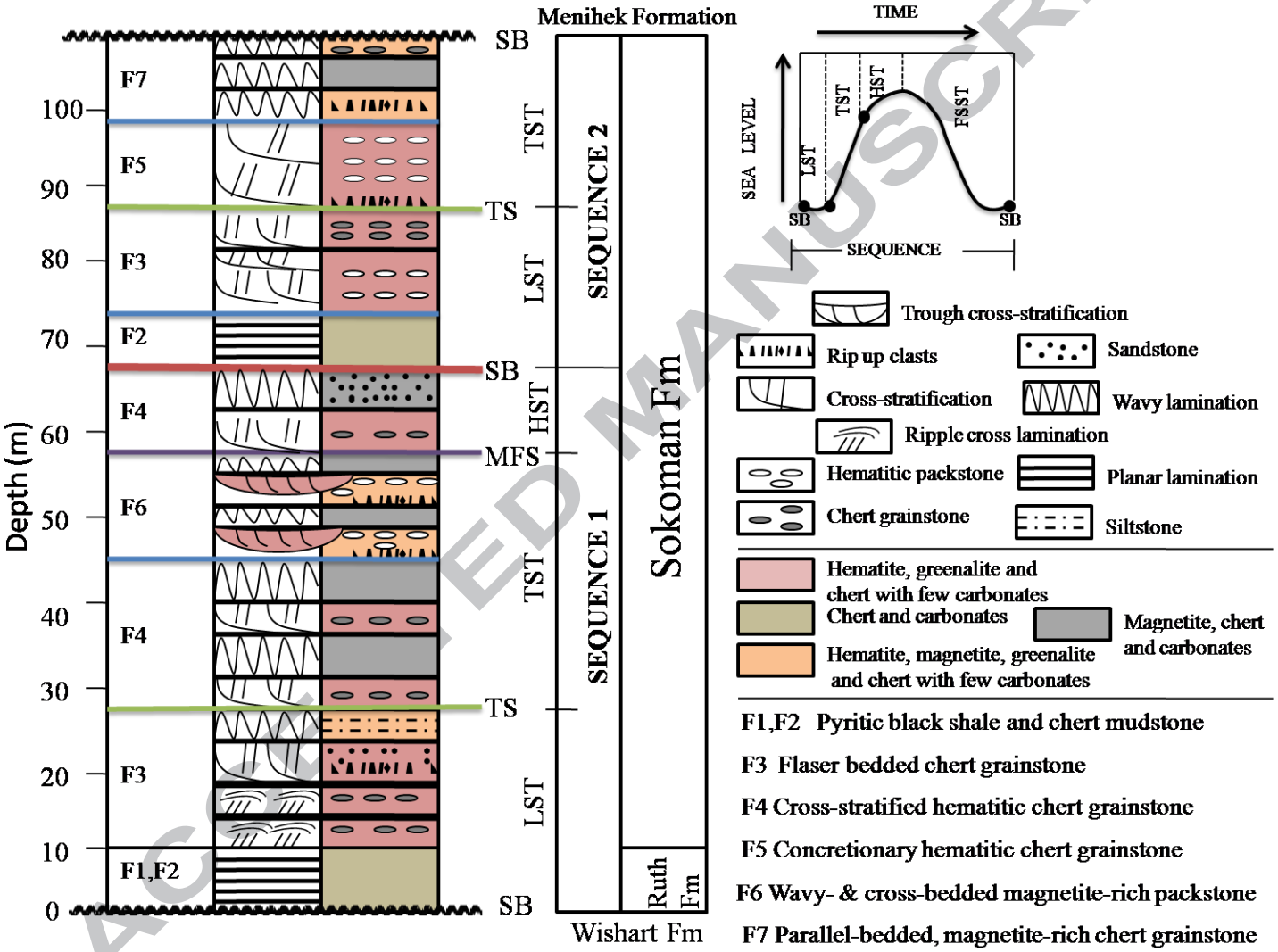

Figure 3

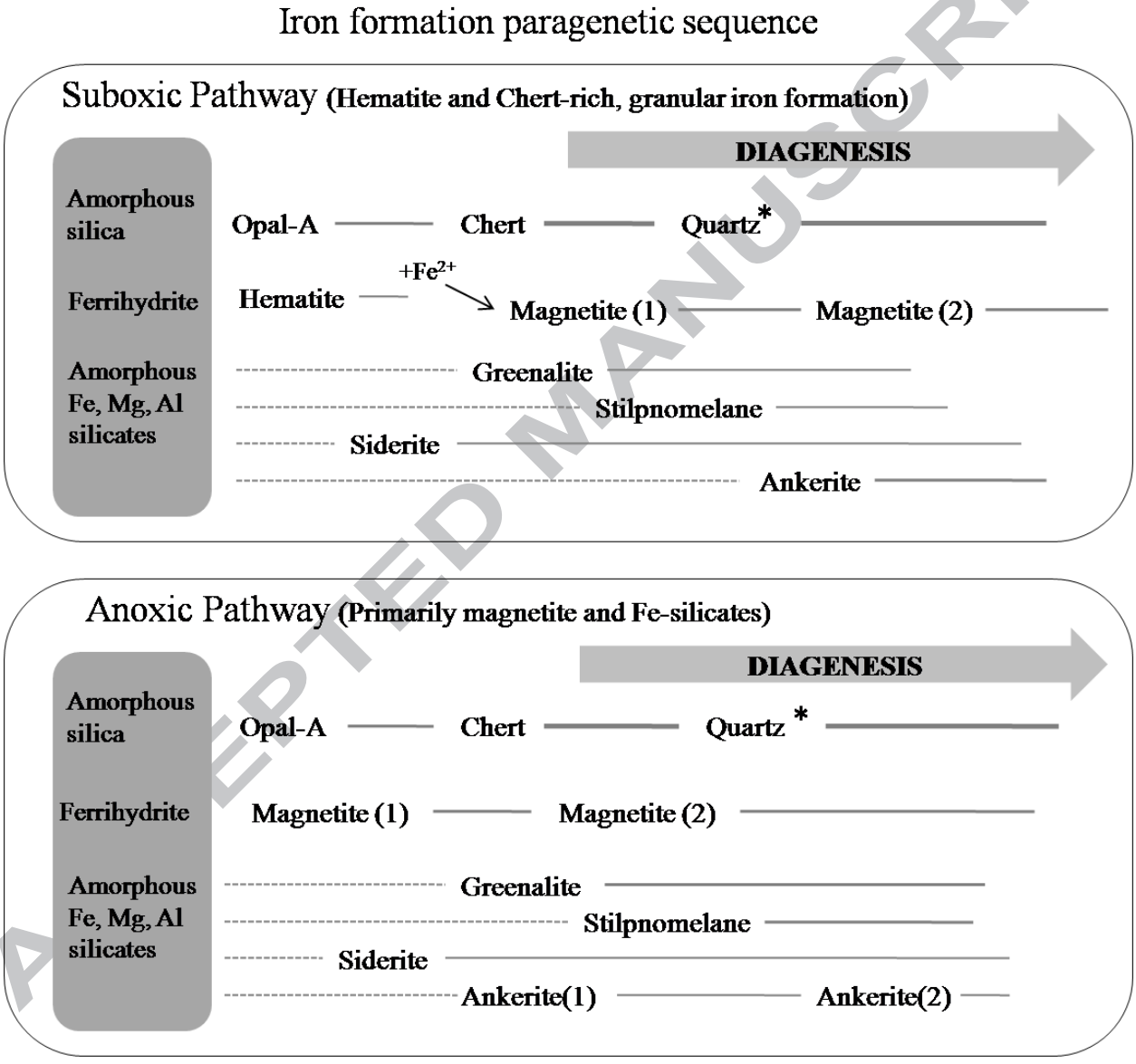

* More than 2 quartz generation

Figure 4

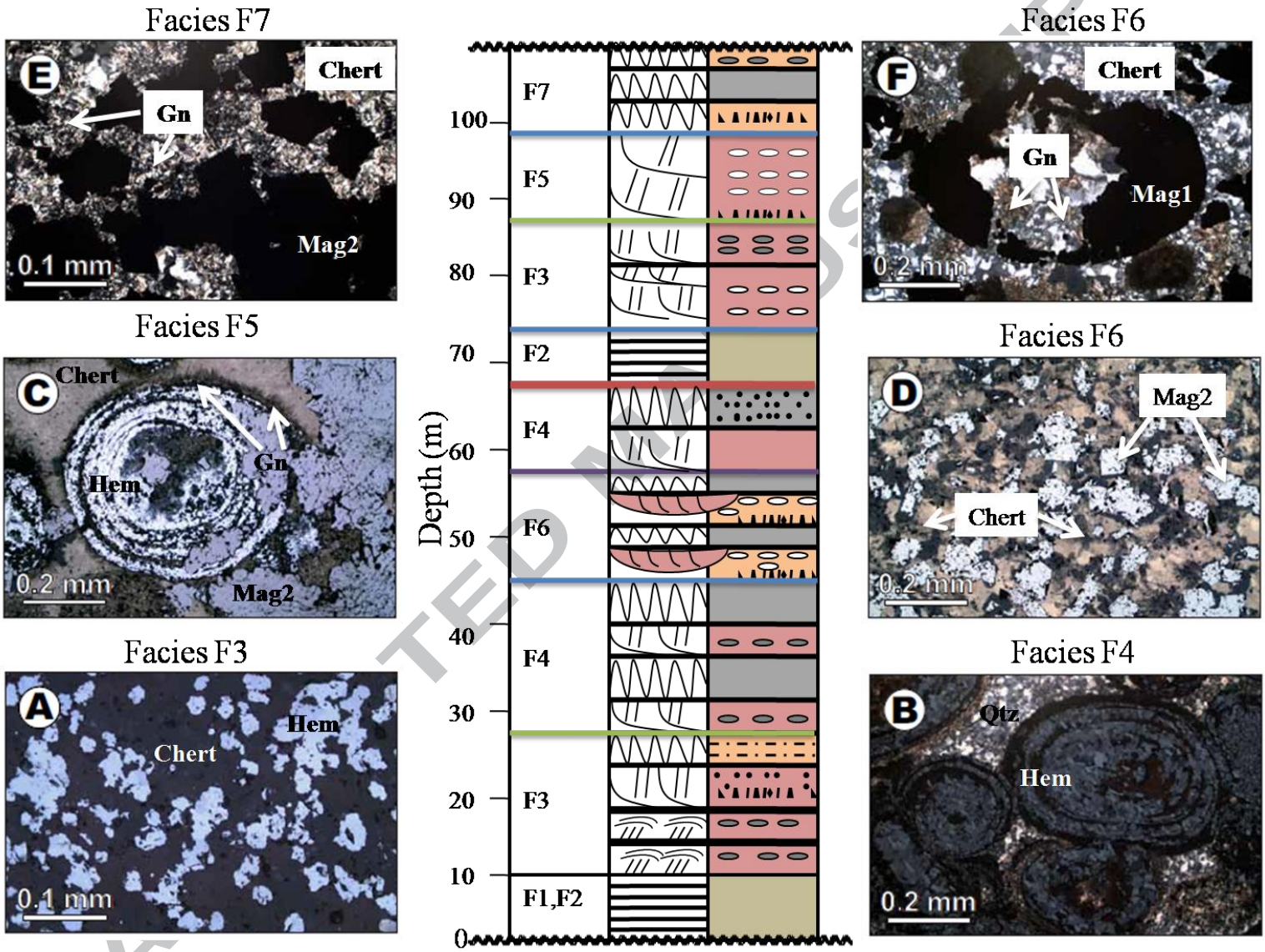

Figure 5

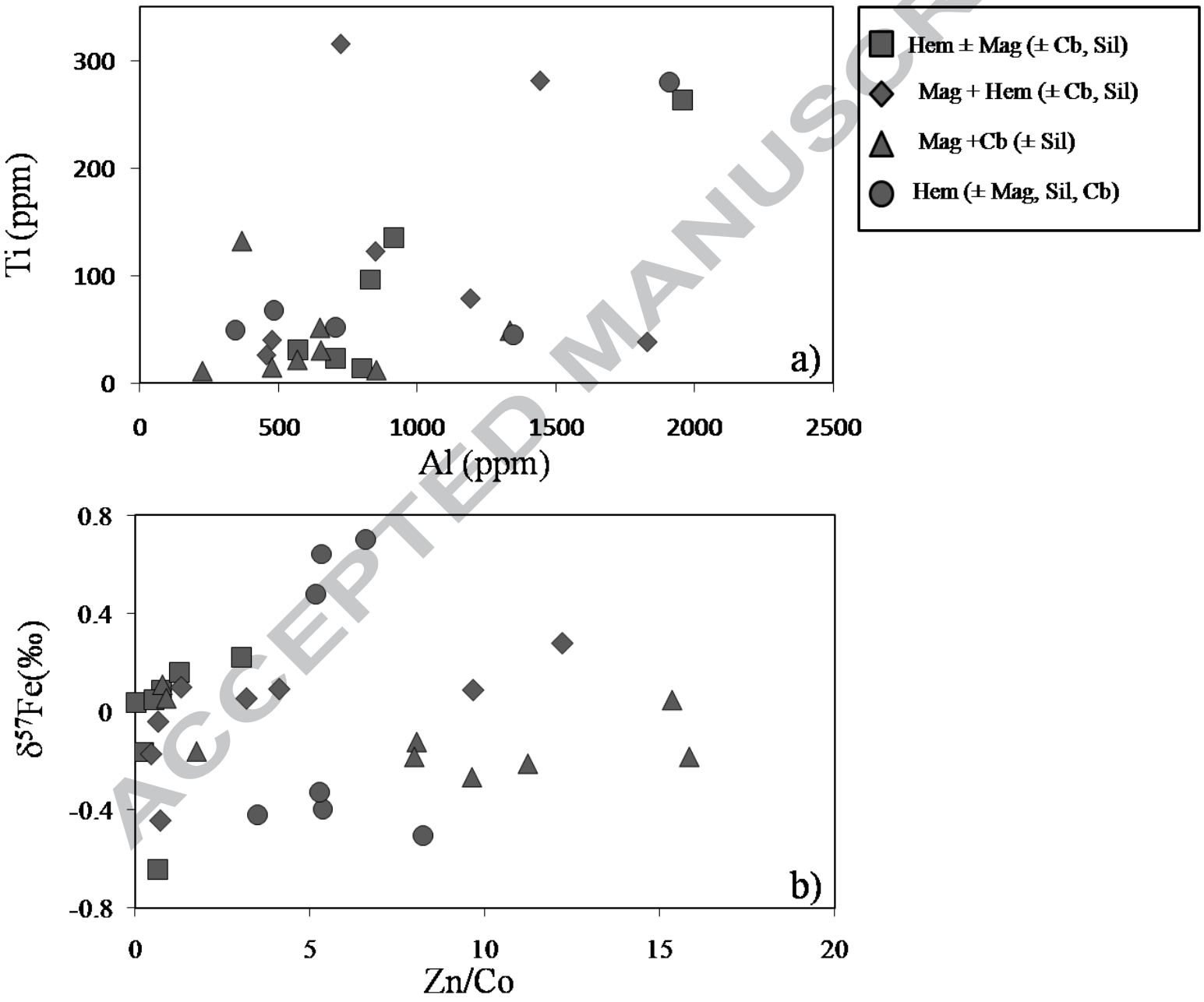

Figure 6

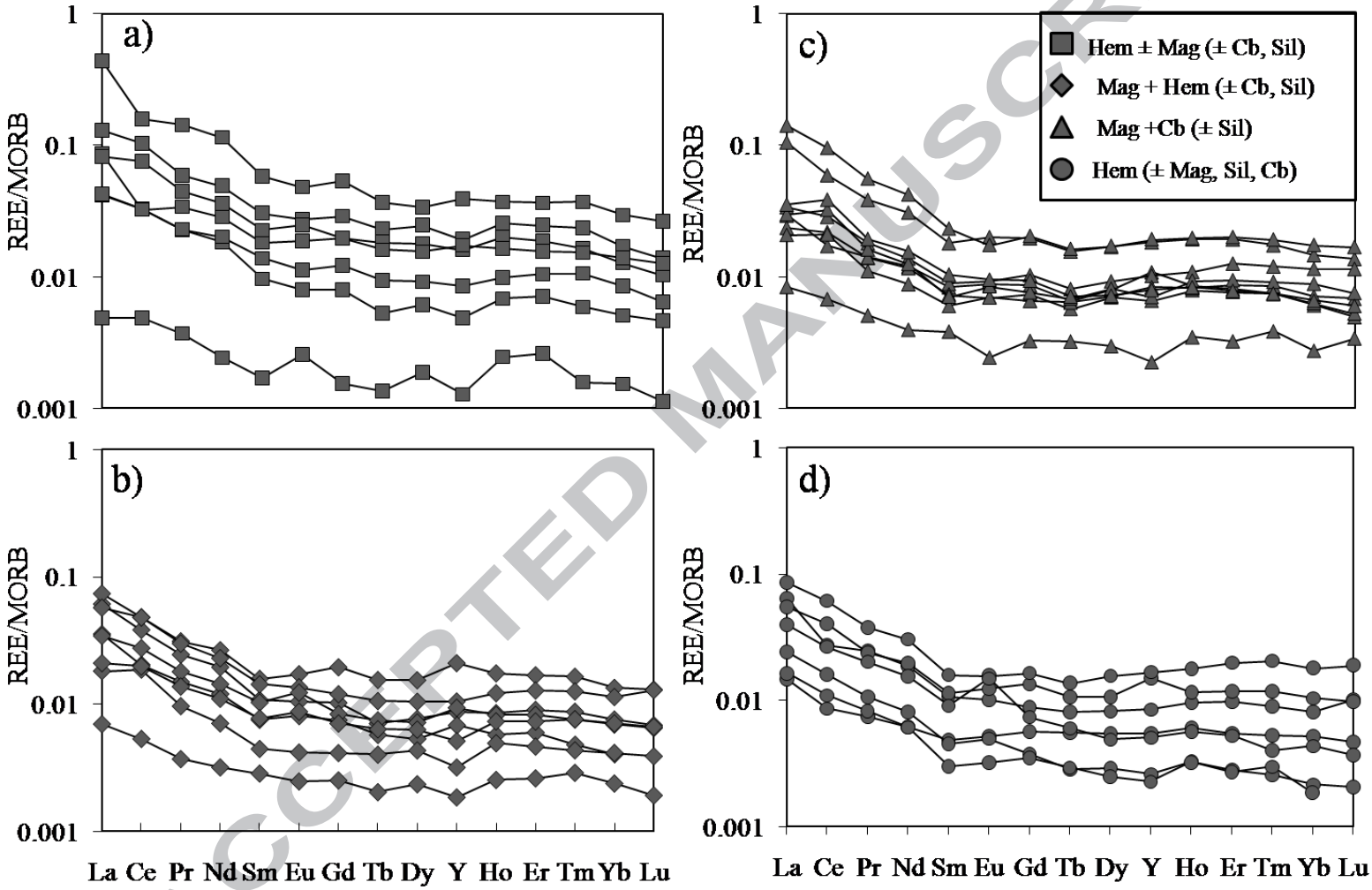

Figure 7

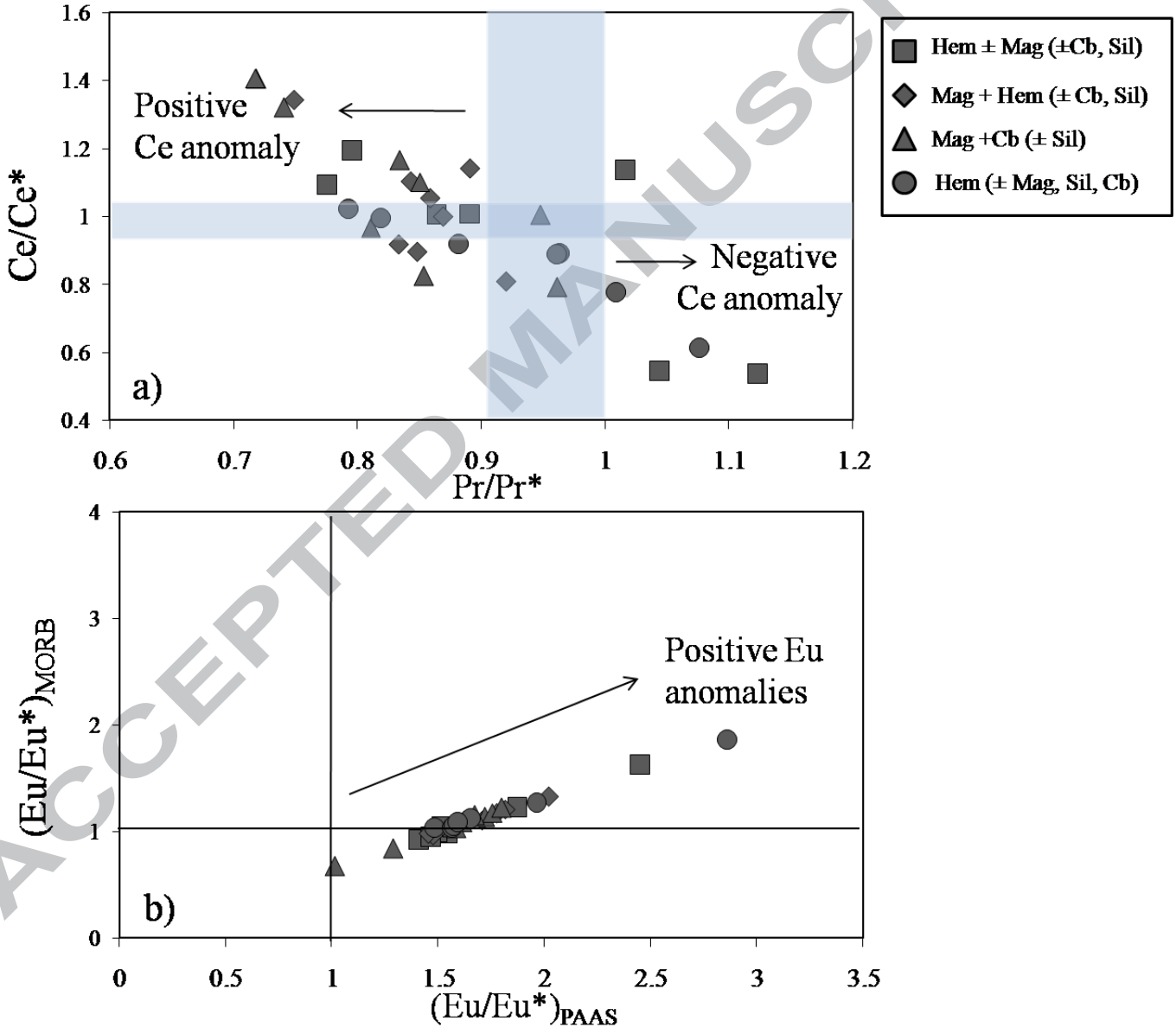

Figure 8

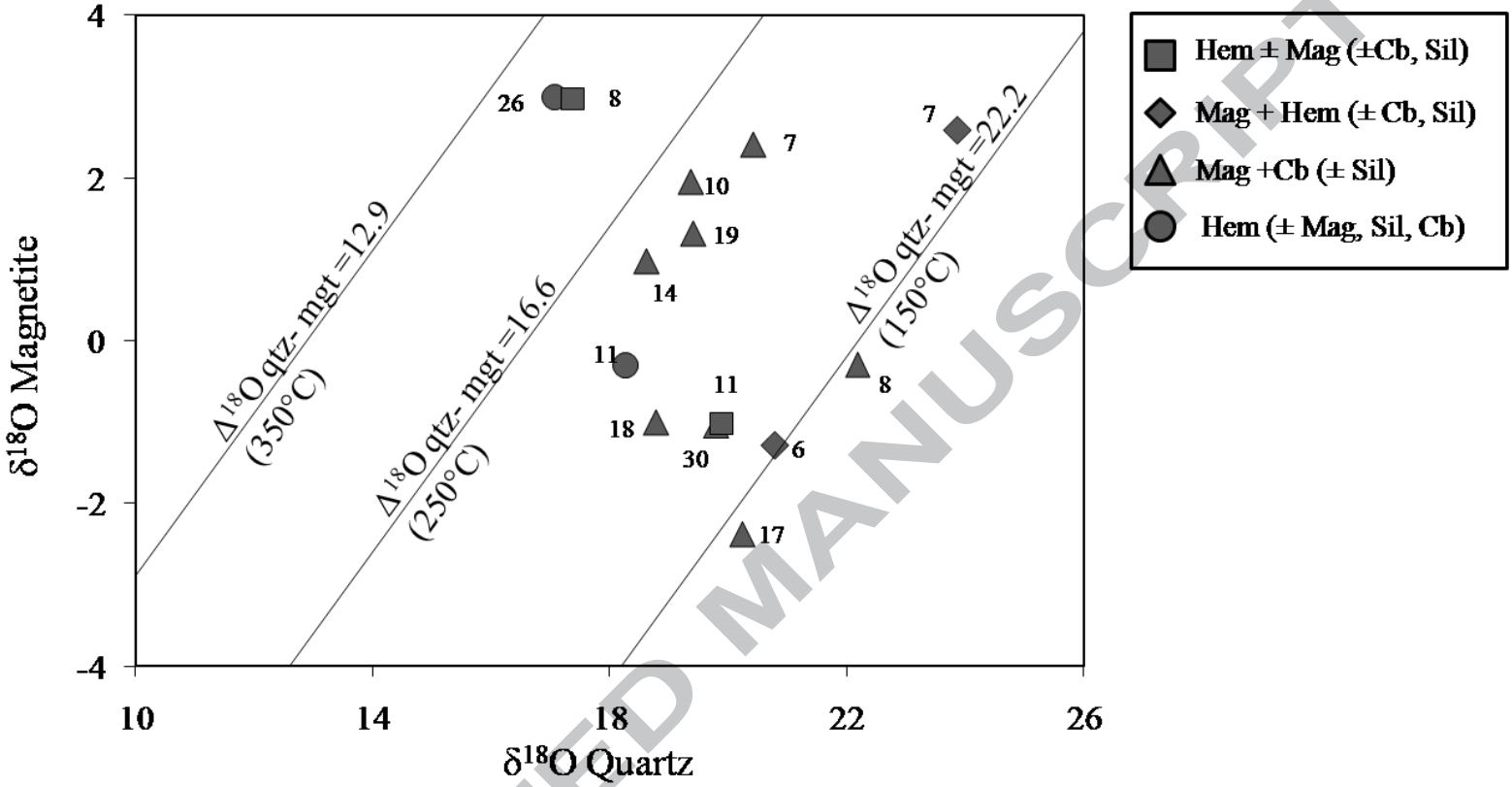

Figure 9

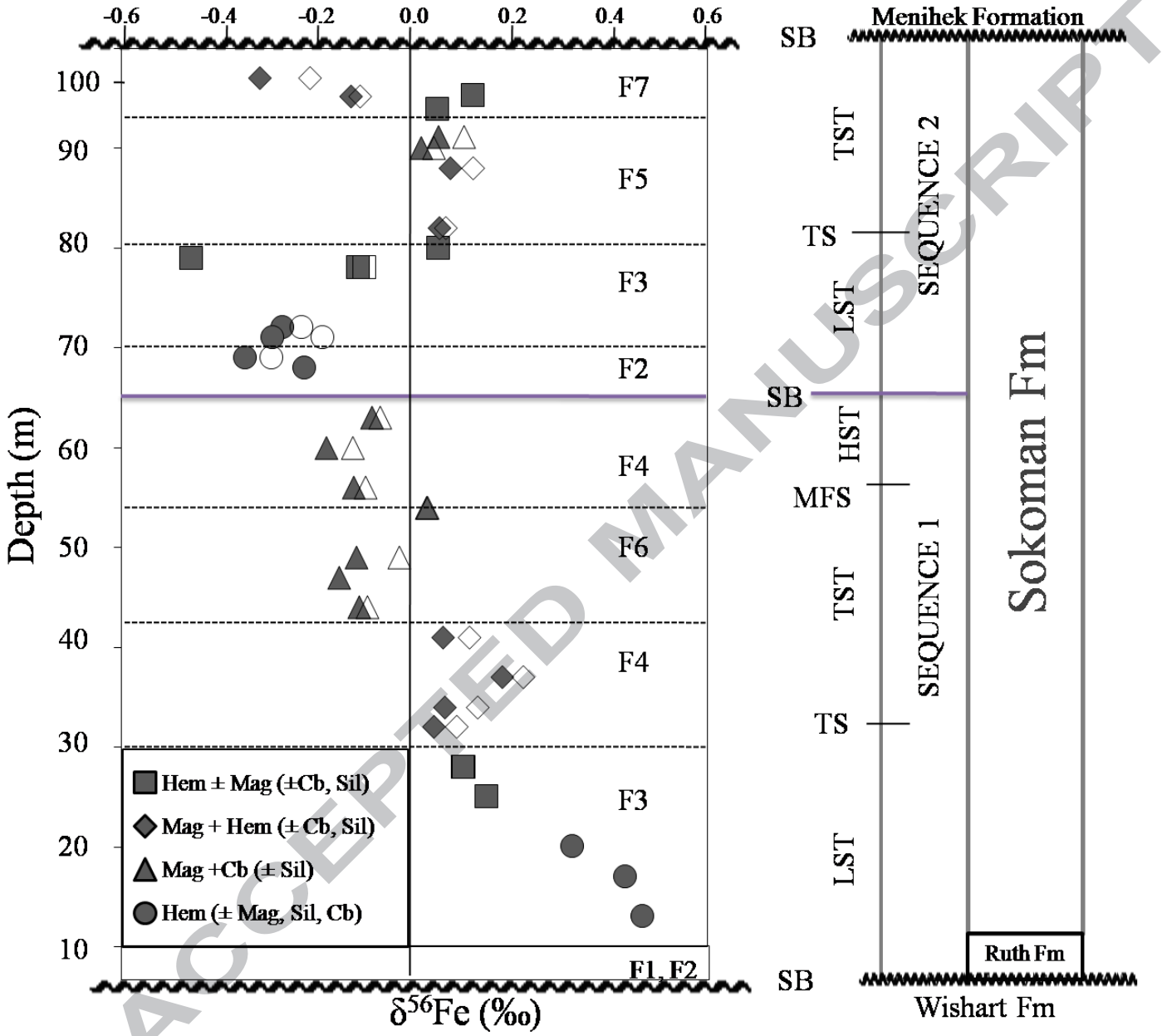

Figure 10

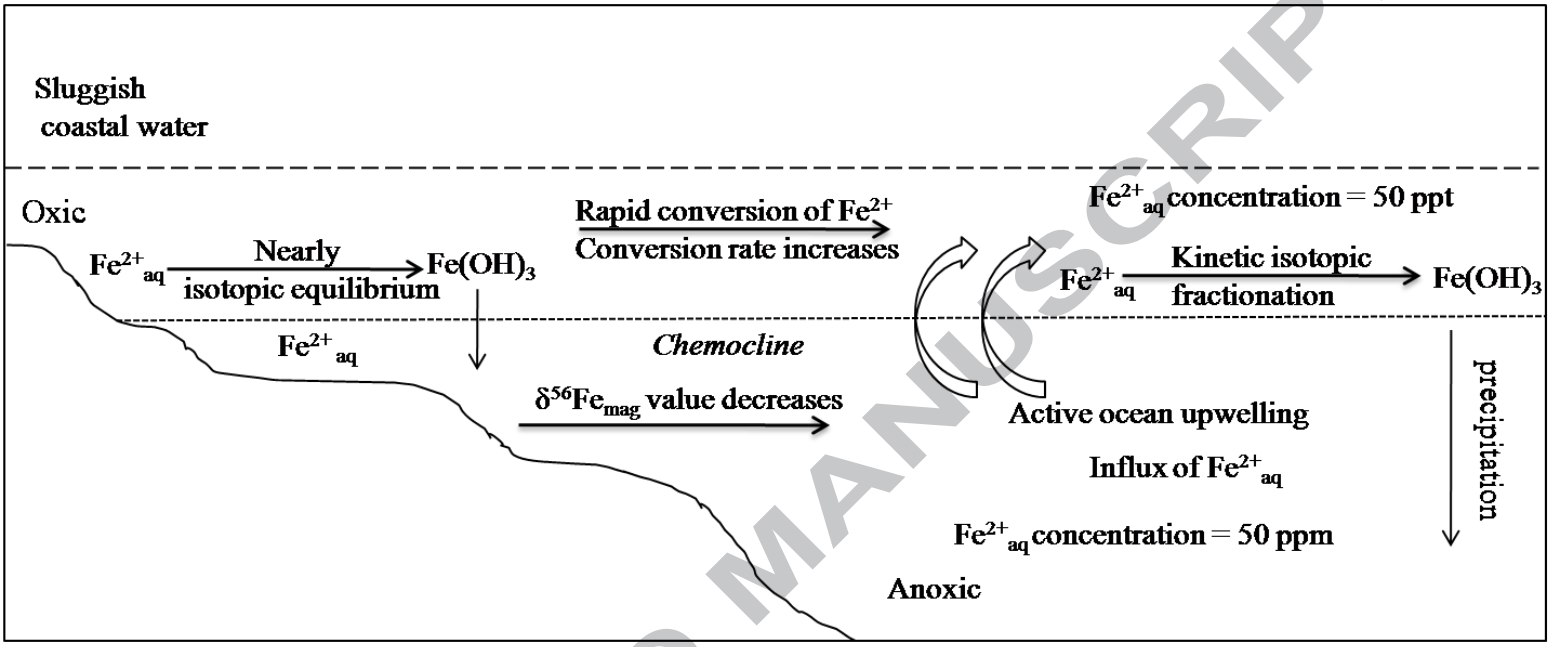

Table 1. $\delta^{18}O$ values of Magnetite (Mag) and Quartz (Qtz), their apparent isotopic equilibration temperatures, and calculated $\delta^{18}O$ values of fluids for samples from the Sokoman Banded Iron Formation. Sample No. refers to drill hole number and depth (m)

Sample no.	$\delta^{18}O$ Mag	$\delta^{18}O$ Qtz	Apparent Temp (°C)	$\delta^{18}O$ fluid
HR1279-8.85	2.4	20.4	220	11
HR1279-10	2	19.4	230	10.5
HR1279-12	-1.3	20.8	150	6.9
HR1279-22	3	17.4	300	11.4
HR1279-29	-0.3	18.3	210	8.3
HR1279-31	3	17.1	310	11.4
HR1279-37	1	18.6	230	9.6
HR1279-40	-2.4	20.2	140	5.7
HR1279-44	-1	18.8	190	7.5
HR1279-46	-1	19.8	170	7.4
HR1279-51	-0.3	22.2	150	7.8
HR1279-56	1.3	19.4	220	9.9
HR1279-66	2.6	23.9	160	10.9
HR1279-72	-1	19.9	170	7.4

Table 2. Iron isotopic data of whole-rock and magnetites from the Sokoman Banded Iron Formation

Whole rock	Minerals	$\delta^{57}Fe_{mean}$	$stdev_{mean}$	$\delta^{56}Fe_{mean}$	$stdev_{mean}$	n	Magnetite	$\delta^{57}Fe_{mean}$	$stdev_{mean}$	$\delta^{56}Fe_{mean}$	$stdev_{mean}$	n
HR1279-3	Mag + Hem (±Cb,Sil)	-0.44	0.1	-0.32	0.07	3	Mgt	-0.31	0.06	-0.21	0.03	2
HR1279-4.7	Hem ± Mag (±Cb,Sil)	0.18	0.13	0.12	0.08	2						
HR1279-4.8	Mag + Hem (±Cb,Sil)	-0.18	0.07	-0.13	0.04	3	Mgt	-0.17	0.05	-0.11	0.04	3
HR1279-6.1	Hem ± Mag (±Cb,Sil)	0.07	0.08	0.05	0.04	3						
HR1279-8.85	Mag+Cb (±Sil)	0.07	0.16	0.05	0.1	2	Mgt	0.15	0.05	0.10	0.03	2
HR1279-10	Mag+Cb (±Sil)	0.02	0.12	0.01	0.07	1	Mgt	0.06	0.08	0.04	0.05	1
HR1279-12	Mag _Hem (Cb,Sil)	0.11	0.28	0.07	0.18	2	Mgt	0.19	0.05	0.12	0.03	2
HR1279-18	Mag _Hem (Cb,Sil)	0.08	0.13	0.05	0.1	1	Mgt	0.10	0.07	0.06	0.06	2
HR1279-20	Hem (±Mag,Sil,Cb)	0.08	0.14	0.05	0.09	2						
HR1279-21	Hem (±Mag,Sil,Cb)	-0.65	0.14	-0.46	0.09	3						
HR1279-22	Hem (±Mag,Sil,Cb)	-0.17	0.08	-0.11	0.04	1	Mgt	-0.15	0.05	-0.10	0.03	2
HR1279-28	Hem (±Mag,Sil,Cb)	-0.40	0.26	-0.27	0.18	3	Mgt	-0.34	0.09	-0.23	0.05	1
HR1279-29	Hem (±Mag,Sil,Cb)	-0.42	0.09	-0.29	0.05	3	Mgt	-0.28	0.09	-0.19	0.06	2
HR1279-31	Hem (±Mag,Sil,Cb)	-0.51	0.13	-0.35	0.08	2	Mgt	-0.42	0.07	-0.29	0.05	1
HR1279-32	Hem (±Mag,Sil,Cb)	-0.33	0.12	-0.22	0.08	2						
HR1279-37	Mag+Cb (±Sil)	-0.12	0.1	-0.09	0.07	1	Mgt	-0.10	0.08	-0.07	0.05	2
HR1279-40	Mag+Cb (±Sil)	-0.27	0.1	-0.18	0.06	2	Mgt	-0.18	0.10	-0.13	0.06	1
HR1279-44	Mag+Cb (±Sil)	-0.19	0.22	-0.12	0.15	4	Mgt	-0.15	0.06	-0.10	0.04	2
HR1279-46	Mag+Cb (±Sil)	0.04	0.11	0.02	0.07	3	Mgt	0.05	0.06	0.03	0.04	2
HR1279-51	Mag+Cb (±Sil)	-0.19	0.13	-0.12	0.08	2	Mgt	-0.04	0.07	-0.03	0.03	2
HR1279-53	Mag+Cb (±Sil)	-0.21	0.12	-0.15	0.09	2						
HR1279-56	Mag+Cb (±Sil)	-0.16	0.12	-0.11	0.08	2	Mgt	-0.13	0.07	-0.10	0.05	1
HR1279-59	Mag _Hem (Cb,Sil)	0.09	0.13	0.06	0.09	3	Mgt	0.17	0.06	0.11	0.04	2
HR1279-63	Mag _Hem (Cb,Sil)	0.28	0.34	0.18	0.24	2	Mgt	0.33	0.07	0.22	0.04	2
HR1279-66	Mag _Hem (Cb,Sil)	0.09	0.14	0.06	0.1	1	Mgt	0.19	0.06	0.13	0.05	2
HR1279-68	Mag _Hem (Cb,Sil)	0.05	0.17	0.04	0.11	2	Mgt	0.15	0.07	0.09	0.03	1
HR1279-72	Hem ± Mag (Cb,Sil)	0.16	0.13	0.10	0.09	1	Mgt	0.17	0.06	0.10	0.04	2
HR1279-75	Hem ± Mag (Cb,Sil)	0.22	0.27	0.15	0.18	3						
HR1279-80	Hem (±Mag,Sil,Cb)	0.48	0.15	0.32	0.1	2						
HR1279-83	Hem (±Mag,Sil,Cb)	0.64	0.1	0.43	0.07	1						
HR1279-87	Hem (±Mag,Sil,Cb)	0.70	0.13	0.47	0.08	2						